University of Stavanger

FACULTY OF SCIENCE AND TECHNOLOGY

MASTER'S THESIS

Study program/specialization: Petroleum Engineering/Natural Gas Engineering	Spring 2019 Open
Author: Anderson Parra Camacho	Anderson Parra C. (signature of author)
Supervisor: Professor Zhixin Yu	
Title of master's thesis: NiFe hydrotalcite-derived catalyst for CO_2 reforming of methane: the impact of calcination and reduction temperature	
Credits (ECTS): 30	
Key words: Dry reforming of methane Hydrotalcite Ni-Fe based catalyst Coprecipitation Calcination-Reduction	Number of pages: 49 Stavanger,15/06/2019

ACKNOWLEDGMENTS

To professor Zhixin Yu for its guidance and direction during the project.

To Huong, Kristian and Dori for all their teachings and patience in the laboratory, this project would not have been possible without your help.

To my fellow master program classmates. It is over, it is done, we did it

To all the friends that I have made here in Norway, all the laughs have made this trip anything but dull.

And specially to my dear family whom I have missed a lot. Gracias por tanto, perdón por tan poco

ABSTRACT

Carbon dioxide (CO_2) emissions has become a major environmental concern for today's society. As energy demand keeps on rising, the transition to cleaner energies is not fast enough to completely reduce greenhouse emissions. Therefore, new solutions must be found. Recently, several researches have been made on one possible solution. Dry reforming of methane (DRM) can utilize methane (CH_4) and CO_2 two of the most important greenhouse gases for producing valuable syngas as a chemical feedstock for industrial applications.

However, DRM process requires a heterogeneous catalyst for its operation and despite the efforts, a suitable catalyst viable from an economical point of view is yet to be found. Recently, studies on Ni-Fe based Hydrotalcite (HT)-derived compounds have presented promising results.

In this study a series of bimetallic Ni-Fe HT-derived catalysts with Ni loading of 20 wt.% and Fe/Ni molar ratio of 0.1 were prepared by coprecipitation at high supersaturation (fast injection method) and calcined at different temperatures. The catalysts were characterized by X-ray diffraction (XRD), nitrogen adsorption-desorption, temperature programmed reduction (TPR), and hydrogen chemisorption. The rise in calcination temperature generated an increase on crystallite size and reduction peak. On other hand, effects on surface area followed a bell tendency.

Calcined catalysts performance over activity and stability at different reduction temperatures were studied for a DRM reaction at a temperature of 700 °C, atmospheric pressure and a gas hourly space velocity (GHSV) of 120,000 $mL.g^{-1}.h^{-1}$. Calcination at 600 °C was found to be the overall best performer achieving the highest conversions with good signs of stability

.

TABLE OF CONTENT

LIST OF TABLES

LIST OF FIGURES

1. INTRODUCTION

1.1 Background

World energy demand is constantly rising due to growing economies and a nonstop increasing population. Climate concerns are a hot topic in our modern society, change to cleaner technologies is being promoted. Natural gas can play an important role in the transition between fossil fuels and renewables energies.

Despite this changes fossil fuels will remain as an important part of world's energy production generating large amounts of carbon dioxide (CO_2), with global warming implications. Therefore, other measurements must be taken to reduce and utilize CO_2 emissions [1]. Carbon capture and utilization (CCU) is one of the new approaches that can help to mitigate these effects [2].

One of CCU technologies is Dry reforming of methane (DRM) a chemical process that uses CO_2 and CH_4. Two of the most important greenhouse gases, as chemical feedstock and converts them into syngas, carbon monoxide (CO) and hydrogen (H_2). The low H_2/CO ratio from this process is convenient for the production of hydrocarbons via the Fischer-Tropsch synthesis, in addition of oxygenated compounds, such as hydroformylation reaction [3].

DRM reaction is highly endothermic, occurs at a temperature of 643 °C and pressure of 1 bar with a catalytic system. The researches on catalyst have been established for decades and yet challenges remain to be solved. The goal is to synthesize a highly active catalyst with good stability and resistance to deactivation generated by carbon deposition and metal sintering. Noble metals such as Rh, Ru are suitable catalysts showing high selectivity and activity for a carbon free operation [4]. Despite the advantages of noble metal-based catalysts, low availability and high costs make this type of catalyst uneconomical for industrial application. It is the main reason that Ni- based catalyst are more attractive to researchers as catalyst for DRM reaction. Generally, Ni-based catalyst have good availability, low cost, and high catalytic activity [5]. The use of different types of materials as catalyst supports, promoters and preparation methods can lead to overcoming carbon deposition and metal sintering for Ni-based catalyst.

Supports also affect metal dispersion or metal particle size. Suitable supports can be resistant to high temperatures and should be able to maintain the metal dispersion during

reaction [6]. Due to its high specific surface area, low price and good basicity alumina (Al_2O_3) is one of the most studied supports for nickel. Especially its α-phase possesses high thermal stability [7]. In addition, magnesium oxide (MgO) has a favorable effect on CO_2 adsorption thanks to its basicity. These beneficial effects can be combined on mixed MgO-Al_2O_3 supports. Reports that addition of MgO into an Al_2O_3 supported Ni catalyst resulted in an increased specific surface area, total pore volume and basicity, thanks to formation of the $MgAl_2O_4$ spinel phase [8]. Bimetallic catalysts have been studied for improving stability, activity and carbon resistance [9], including noble metals [10]. The use of Fe has been reported with positive results for reducing carbon deposition in some studies, and is also being considered as a suitable promoter [11].

The catalytic activity depends on the support preparation method, reaction conditions and on the pre-treatment of the catalyst before DRM reaction. Hydrotalcites (HT), also called double layered double hydroxides (LDHs), are promising reforming catalyst precursors, as it possesses a homogeneous elemental distribution and high surface areas [12]. After calcination, it forms spinel which generates a high thermal stability. It is promising materials for many applications, due to a large variety of compositions, low cost and various preparation parameters that can tailor suitable catalytic structures for specific requirements. After a controlled thermal decomposition, homogeneous mixed oxides with high surface areas are obtained, which are thermally stable.

1.2. Scope of the study

The objective of this work was to study the effect of calcination and reduction temperatures on catalytic activity and stability of bimetallic Ni-Fe HT-derived catalysts in DRM reaction.

A series of bimetallic Ni-Fe HT-derived catalysts with Fe/Ni molar ratio of 0.1 were prepared by coprecipitation at high supersaturation (fast injection method). The catalysts were characterized by X-ray diffraction (XRD), nitrogen adsorption-desorption, temperature programmed reduction (TPR), and hydrogen chemisorption. The catalysts were tested in DRM reaction at a temperature of 700 °C, atmospheric pressure and a gas hourly space velocity (GHSV) of 120,000 $mL.g^{-1}.h^{-1}$ at different reduction temperature over catalysts calcined at different calcination temperatures.

2. LITERATURE REVIEW

2.1 DRM reaction thermodynamics

DRM is a complex system governed by the reaction between CH_4 and CO_2, where simultaneously several side reactions are also present in the process. main and side reactions are shown in table 2.1[13].

A thermodynamic analysis is necessary to define the most suitable conditions for a reaction, such as temperature, pressure, reactants compositions, etc. Determination of optimum operating conditions by study of carbon formation boundary provides a fundamental remedy to prolong the catalyst lifetime and to surpass the performance of the reaction system [14]. Minimizing carbon deposition is a matter of special interest because it is the main cause for catalyst deactivation and a huge problem for the industrial application of DRM.

Table 2.1 Thermodynamic analysis of main and side reactions

Reaction	Equation	ΔH_{298K} (KJ/mol)	T (°C) $\Delta G° \leq 0$
Dry Reforming of Methane	$CH_4 + CO_2 \leftrightarrow H_2 + CO$	+247	≥ 643
CH_4 Decomposition	$CH_4 \leftrightarrow C + 2H_2$	+75	≥ 546
CO Disassociation (Bouduard Reaction)	$2CO \leftrightarrow CO_2 + C$	-171	≤ 703
Reverse Water Gas Shift (RWGS)	$CO_2 + H_2 \leftrightarrow CO + H_2O$	+41	≥ 827
CO_2 Gasification	$C + CO_2 \leftrightarrow 2CO$	+171	≥ 703
Carbon Water Reaction (CW)	$C + 2H_2O \leftrightarrow 2H_2 + CO_2$	+90	≥ 631

The enthalpy change of the main reaction is +247 KJ/mol which indicates a very endothermic reaction that requires large amount of heat input. According to thermodynamic principles when $\Delta G° \leq 0$ a reaction occurs spontaneously, and when $\Delta G° \geq 0$ the reaction is thermodynamically limited. As for DRM reaction, it will occur spontaneously at 643 °C. The reactant fractions will decrease with increasing temperature given the endothermic nature of the process. Carbon deposition is of special interest because it is the main cause for catalyst deactivation and a challenging problem for the industrial application of DRM. It is known to be affected by thermodynamics and CH_4 decomposition and CO disassociation is considered to happen. The result from the analysis show that CH_4 cracking occurs at T ≥ 546 °C, a slightly endothermic behavior. CO disassociation on the other hand occurs when T≤703 °C. Deposited carbon can also

be consumed by CO_2 gasification that takes place at T≥703 °C and by carbon water reaction (CW) at T≥631 °C. Based on the results, that severe carbon formation is happening between 546 °C and 703 °C. This temperature range should be avoided. Reverse gas water shift is important because it consumes H_2 to produce water. However, this consumption will affect the product ratio and is the main reason for a low H_2/CO ratio. As for the DRM reaction, it is not recommended to produce H2 because it is not desirable for RWGS reaction to happen [15]. According to Cao *et al.* [13], DRM reaction is endothermic and favored over 827 °C and the appropriate conditions for a low carbon regime are given at T ≥ 1000 °C.

In the same study, it was shown that high pressure was unfavorable for high conversion of CH_4 and CO_2 conversion purposes. This can be explained according to Le Chatelier's principle, ideal pressure for reaction was found to be 1 bar (0.1 MPa) with a CH_4/CO_2 ratio of 1:1 [13].

2.2 Catalyst for dry reforming of methane

The catalytic activity and stability of the catalyst are highly influenced by different type of active metal, support, promoter selection, calcination temperature, preparation method, and reactor type [16].

2.2.1 Nickel based catalyst

A majority of group VIII metals have been studied and identified as suitable supported catalyst for DRM. Among them, noble metals show the overall best qualities with high activities and selectivity for a carbon free operation [17]. However, their limited availability and high cost has prevented their commercial use for industrial applications. Ni-based catalyst has been intensively studied as the most promising catalytic system for DRM reaction due to its high catalytic activity, lower price and good availability.

Nevertheless, Ni-based catalyst are not exempt of problems and have a high tendency to coke formation because nickel also catalyzes carbon deposition [18]. Enhanced catalytic stability has been the focus of extensive studies, by using different type of promoter, different supports and various preparation methods. Metal sintering is also a problem due to reaction occurring at high temperatures for nickel, above Tammann temperature (for Ni that is 600 °C) [19]. Several studies have reported the effect of particle size on activity and carbon deposition, large particle size reduces catalytic for activity and accelerates carbon formation rate [20, 21].

2.2.2 Catalyst supports

Catalyst performance is influenced by the support. Support materials provide resistance towards carbon formation and maintain the high dispersion of the catalyst. High surface area and porosity are also desirable to obtain a higher activity. Furthermore, the interaction between the support and the active metal plays a crucial role on the catalyst´s reducibility and stability.

Numerous factors that affect catalytic performance should be considered during catalyst design, such as surface area, thermal stability, pore characteristics, redox properties and surface basicity [3]. Suitable choices in catalyst preparation and activation methods/parameters will enhance the metal-support interaction, improve active metal dispersion, hinder sintering, ease catalyst reduction and reduce carbon deposit rate [22].

For Ni-based catalyst a commonly researched support is Al_2O_3 that is relatively cheap, offers a basic character and good specific surface area. Studies made by Ashok *et al.* [23] and Guo *et al*. [6] have shown that addition of MgO to Al_2O_3 in a Ni-based catalyst helps to prevent the formation of $NiAl_2O_4$ spinel phase which is inactive and leads to a low metal dispersion of NiO/Al_2O_3. When comparing $Ni/\gamma\text{-}Al_2O_3$, $Ni/MgO\text{-}\gamma\text{-}Al_2O_3$, and $Ni/MgAl_2O_4$ during DRM reaction, it was found that $Ni/MgAl_2O_4$ is more stable and have higher activity. MgO modification of alumina is key to increase metal dispersion due to its ability to weaken the NiO-alumina interaction.

According to Wu *et al*. [10]. The enhanced metal-support interaction to Al_2O_3 provided by MgO allows keeping a small Ni particle size to hinder metal sintering. Authors concluded that the better coke resistance from $Ni/MgAl_2O_4$ compared to Ni/Al_2O_3 was because MgO basic sites on catalyst´s surface helped to improve CO_2 adsorption causing a faster carbon gasification.

The catalytic activity also depends on the support preparation method, reaction conditions and on the pre-treatment of the catalyst before DRM reaction. Min *et al.* [8] reported that coprecipitated $Ni\text{-}MgO\text{-}Al_2O_3$ catalyst with larger crystallite size was deactivated faster than catalysts with smaller crystallite size (prepared by sol-gel method). It was supposed that sintering of Ni particles occurred in this case.

2.2.3 Bimetallic Ni-based catalysts

Among the different options that have been researched for improving Ni-based catalysts stability, one that have had interesting results is the addition of a secondary metal to Ni.

Researchers have investigated alloy-catalyst to overcome economical and operational problems presented by noble and non-noble based catalysts. Given the excellent performance of noble metal catalysts in activity and stability, small amounts of these metals have been tested as secondary metal (Pt, Rh, Ru, Pd). Besides non-noble metals such as (Fe, Co, Mn) have also been tested. In both cases an improvement over carbon resistance, stability and activity was achieved compared to monometallic catalysts [9].

From an economic perspective Fe is a promising candidate as is much cheaper than Ni [24], and Ni-Fe alloy catalyst has shown better stability and higher activity level than Ni monometallic catalyst. According to Galvita *et al.,* carbon is formed mainly on Ni surface during dry reforming reaction [25]. Methane will decompose over Ni, forming hydrogen and carbon. Metallic Fe will be separated from the alloy in the presence of CO_2 to form FeO_x. Afterwards, oxygen will migrate from FeO_x to a Ni atom, oxidize the carbon that was formed from methane decomposition and generate CO, helping to decrease the carbon deposition process.

The Ni/Fe ratio is of great importance for Fe effect on Ni-Fe/$MgAl_2O_4$ catalyst activity for the DRM reaction. According to Theofanidis *et al.,* Ni-Fe alloy is stable for reductions up to 627 °C, but at higher temperatures, it will break down to Fe_3O_4 and metallic Ni for a Fe/Ni molar ratio of 0.7 [11].

2.2.4 Hydrotalcite (Layered Double Oxides)

Hydrotalcite is a layered mineral with chemical formula $Mg_6Al_2(OH)_{16}CO_3{\cdot}4H_2O$ that can be found in nature. Nowadays the term is also employed to identify a variety of synthetic and natural compounds (layered double hydroxides-LDH) that have a layered structure similar to hydrotalcite-like materials [26]. LDH are quite promising for several applications, due to low cost, a large variety of compositions and a wide range of preparation variables that provides customized materials for specific requirements.

Hydrotalcite layers are made of octahedral units, where a divalent or trivalent cation is in the center of an octahedron and six OH^- groups are placed in the corners. Similarly, to brucite, this units are linked by edges, forming parallel layers. Arrangement of the layers can determine hexagonal or rhombohedral symmetry of the hydrotalcite structure, in which the unit cell is built up from three and two hydrotalcite layers, respectively. Rhombohedral symmetry is generally more common [7].

General formula LDH compounds is

$$[M^{2+}_{1-x}M^{3+}_{x}(OH)_2]\,[(A^{n-}_{x/n})\cdot mH_2O]$$

Where M^{2+}, M^{3+} are di-valent and tri-valent cations; A represents interlayer anions and x represents trivalent cations mole fraction. Brucite-like layers are described in the formula by $[M^{2+}_{1-x}M^{3+}_{x}(OH)_2]$ and interlayer composition is then described by $[(A^{n-}_{x/n})\cdot mH_2O]$. From experimental results, the suggested x value is between 0.2-0.33. Out of this range, hydroxides or other compounds may be formed [27].

In the positive-charged brucite-like layers, magnesium cations (Mg^{2+}) has been partially replaced by aluminum cations (Al^{3+}). In the interlayer spaces, anions are present compensating this charge. Voids in the spaces are completed by water molecules giving completion to the HT structure. A graphic representation is given in figure 2.1 [7].

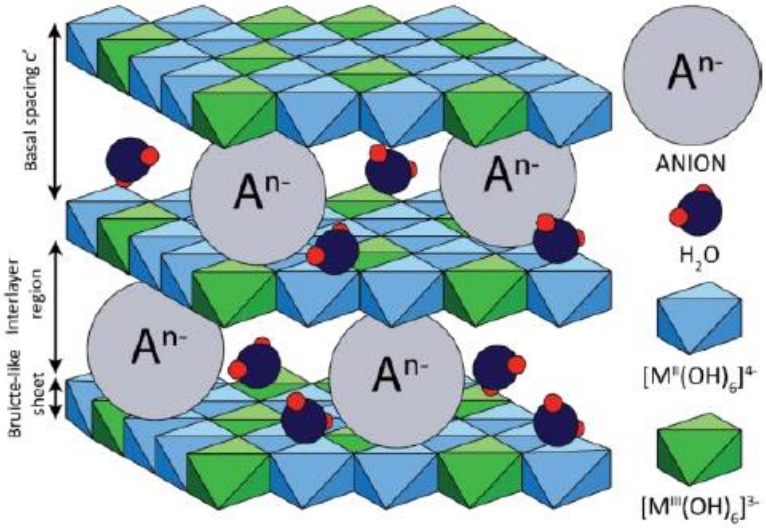

Figure 2.1 Schematic representation of hydrotalcite structure [7]

Several components can replace Mg^{2+} and Al^{3+} as the divalent and trivalent cations for a hydrotalcite-like material due to possessing a similar ionic radii [27]. For this study Ni^{2+} and Fe^{3+} are chosen.

2.2.5 Catalyst synthesis

Different synthesis techniques such as titration, precipitation (high and low supersaturation), hydrothermal treatments, supported HT and HT preparation with anions other than carbonates have been researched [12].

One of the most popular methods for LDH synthesis is coprecipitation where parameters such as metal concentration, pH, rate of addition, mixing efficiency, ratio of anions and cations are of great importance.

HT like other catalytic materials, can be reduced to nanoscale dimensions. Nanoparticles can present size-related properties significantly different from those of either bulk materials or fine particles. This can be attributed to a large surface area and can affect their catalytic performance [28].

2.2.5.1 Coprecipitation

Coprecipitation is one of the most common direct synthesis methods. This process involves nucleating and growing the metal hydroxide layer by mixing an aqueous solution which contains two metal ions in the presence of a base and the desired anion. Limitations of this method includes that the anion to be incorporated in LDH should not form insoluble salts with constituent cations easily. Therefore, LDH phosphates cannot be synthetized by this method. Besides it can only be implanted if the interlayer anion is at least held as firmly as the counterion in the metal salts used. Hence, sulfates should be avoided while metal chlorides and nitrates are widely used [27].

Certain measures can be taken for improving synthesis such as precipitation at constant pH with all cations precipitating simultaneously in a fixed ratio. A simultaneously steady addition of a solution of base and a solution of cations under strong stirring is also required to prevent aggregation of poor crystallinity. Rates of addition must be regulated for a steady pH. The selected pH must be above LDH formation level, but also below the required level required for divalent metal hydroxide precipitation [27]. According to Bhattacharyya [29] this pH range is between 7 and 10.

Different coprecipitation methods have been researched, in this study coprecipitation at high supersaturation at constant pH will be utilized. For coprecipitation at room temperature, the process is determined by growth mechanism and nucleation. Adding the metal precursor at a high rate, fast injection by a syringe, forms several nucleation sites

while growth is been restricted by the absence of free metal precursor. In this method small particles with a narrow particle size distribution will be formed [30]. These results are in accordance to Nyvlt *et al.* [31] giving that higher nucleation rates form larger number of nuclei and a smaller crystallite size.

2.2.5.2 Aging

Aging step, vigorous stirring under a determined temperature for a given time, is a vital part for catalyst synthesis with great influence on its morphology [31]. During aging crystal growth is enhanced, the smaller particles get dissolved back in the solution and take part in growth of bigger particles, this process is believed to occur by the Ostwald ripening mechanism [32], the number of stacked layers is increased.

It is worth mentioning that layer stacking is enhanced after aging regardless of the synthesis procedure [31]. According to Wang *et al*. [33] grain shape and size are dependent on aging temperature; a bigger size and a more regular hexagonal shape were found when increasing temperature from 50 °C to 90 °C.

2.2.5.3 Calcination

Despite different composition for many hydrotalcite-like materials, they possess a similar behavior for thermal decomposition [26]. Products from LDHs decomposition have several applications not only in DRM catalysis but also in different industrial applications.

Generally, calcination process has four steps proceeding at different temperatures ranges

I) Below 100 °C: Adsorbed water removal from crystallites external surfaces

II) 100 °C-250 °C: Interlayer water removal

III) 250 °C-500 °C: Hydroxyl groups removal as water vapor from LDH layers

IV) 250 °C- 500 °C: Interlayer anions decomposition.

As can be seen from temperature ranges, steps III and IV usually occur simultaneously [34]. Calcination at high temperatures is usually associated with a 40% loss of catalyst initial weight as reported in several studies for a variety of LDH compositions [12, 35, 36] . Due to this, hydrotalcite structure collapses and hydroxide materials become mixed oxides with well dispersed cations.

Water and other gaseous products from decomposition that are released by calcination from the LDH structure can create channels in brucite-like layers promoting extra porosity. Hence a higher surface area from mixed oxides by calcination will be obtained compared to the original hydrotalcite material before the thermal treatment [12].

With additional heating (700 °C), further structural changes may occur in the mixed oxides periclase-like structure giving as a result a stable spinel phase formation. For some materials such as $MgFeCO_3$ this process can occur at lower temperatures (350 °C) forming the $MgFe_2O_4$ spinel [26]. Showcasing the importance of selecting an appropriate calcination temperature for a good catalytic activity on DRM [7].

2.2.5.3 Reduction

For catalyst to be active, an additional process is needed. Hence, reduction is considered the catalyst activation step. By using a reducing agent, the mixed oxides present in the catalyst will be reduced and transformed into active metallic species. The reduction process is mainly dependent on temperature which have an impact on metal surface area, dispersion and extent of reduction of the catalyst. It is reported that increasing calcination temperature, before reduction, will decrease reducibility [12].

2.3 Catalyst characterization

2.3.1 X-ray Diffraction (XRD)

X-ray powder diffraction is one of the main characterization techniques in catalysis analysis, employed to determine crystalline materials atomic structure without the necessity of large single crystals (100 μm). Films grown on a substrate or polycrystalline phases can be analyzed with this technique [37].

When an incoming X.-ray hits a powder sample, waves are scattered by the atoms in a lattice, photons that are scattered will interfere at distinct angles, then a detector will record a pattern of contrasting intensities as a function of diffraction angles. This can be described by Bragg law [38]:

$$\lambda = 2 \times d \times \sin \theta \qquad (2.1)$$

where λ is the electromagnetic radiation wavelength (Å), d the distance between lattice planes of atoms and θ is the angle of incidence between x-ray beam and the lattice plane. Note that the angle of deviation of the x ray is 2θ from its initial direction.

Peaks position in the patterns of diffraction enclose information about crystalline phases in the sample. Shape and width of the peaks provide data on crystal microstructure. An estimate of crystallite size (d) can be calculated by using Scherrer equation [39].

$$d = \frac{K\lambda}{B\cos\theta} \qquad (2.2)$$

Where *B* is the full width at half maximum (FWHM) of the peak (radians) and *K* is the crystallite shape factor. Most of x-ray diffractometers use Cu or Mo as the metallic target for the x-ray tube. Cu *K* value is 1.5418 Å.

Intensities and positions of peaks from XRD can be compared to a known materials database for identifying sample content and presence or absence of a particular phase [37].

2.3.2 N_2 Adsorption-desorption

One of the various experimental methods for characterization of pore size and surface area is gas adsorption. This method allows a wide range of pores sizes assessment (0.35 nm to 100 nm) and is not cost intensive when compared with other alternatives. Adsorption processes can be classified in two categories according to the strength of the interaction: chemisorption and physisorption. From the two, physisorption is the most convenient for surface area measurement due to low heat of adsorption with no structural change to the surface during measurement. Besides, no activation energy is necessary so adsorption equilibrium can be achieved quickly. Physisorption is fully reversible which allows an analysis on adsorption-desorption processes. Unlike chemisorption surface may be covered by more than one layer of adsorbate. Moreover, adsorptive can fill pores completely for pore volume measurements used for pore size and distribution calculations [40].

The Brunauer–Emmett–Teller (BET) gas adsorption method has become the main standard procedure for surface area determination of porous materials. Basically, the Langmuir adsorption isotherm approach is extended to multilayer adsorption and BET equation is formulated:

$$\frac{P}{V(P_O-P)} = \frac{1}{V_mC} + \frac{(C-1)P}{V_mCP_O} \qquad (2.3)$$

Where: V is the volume of gas adsorbed at pressure P, V_m is the volume of gas adsorbed in monolayer, P_O is the saturation pressure of adsorbate at experimental pressure (-196°C for N_2) and P/P_O is the relative pressure. C is a constant relate to the heats of adsorption and liquefaction of the gas.

If BET equation is satisfied, plotting of $P/V(P_O - P)$ vs P/P_O would give a straight line where V_m can be evaluated using the slope and the intercept. Thus, for relative pressure (P/P_O) values between 0.05 and 0.3 a calculation of surface area can be performed. [41].

According to IUPAC (International Union of Pure and Applied Chemistry) classification, physisorption isotherms can be divided in six types, from type I to type VI [42], as shown in figure 2.2.

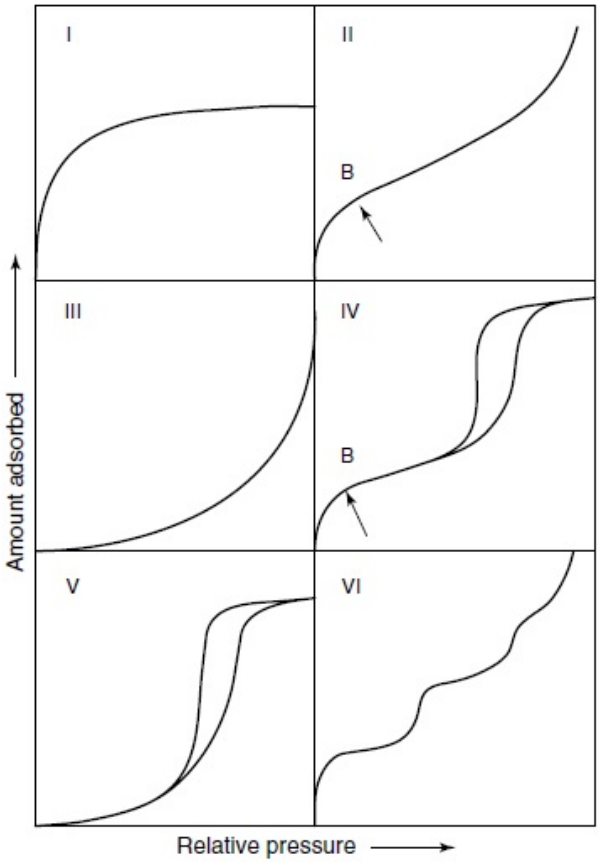

Figure 2.2 Types of physisorption isotherms [42]

One of the most important are the Type IV isotherms, usually observed in many industrial adsorbents with a mesoporous structure (pores between 2nm to 50 nm). It has a characteristic hysteresis loop with limiting uptake over a range high P/P_O values. Thus, hysteresis loops have their own classification over a wide variety of shapes as shown in figure 2.3.

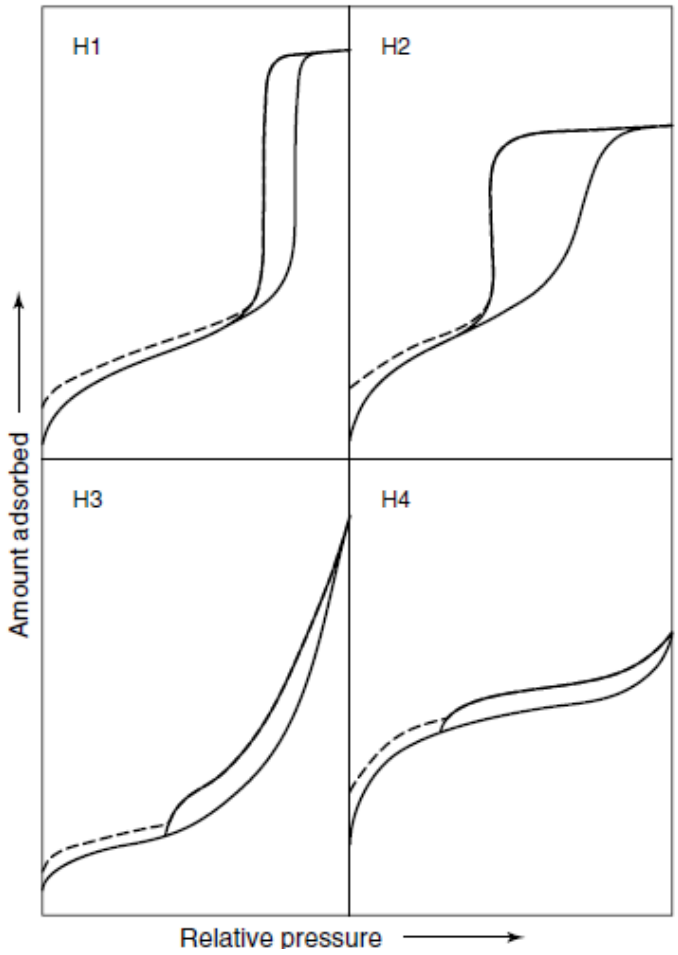

Figure 2.3 Types of hysteresis loops [42]

Shapes of hysteresis loops are associated with specific pore structures, Type H1 for example is often found on porous materials that consist of agglomerates in a regular array of uniform spheres which have a narrow pore size distribution. Type H2 is difficult to interpret for porous adsorbents given that in those systems pore size and shape are not properly defined [42].

One of the methods for mesopore size analysis is Barrett- Joyner - Halenda (BJH), which use a modified Kelvin equation combined with the gas desorption isotherm to determine pore size and pore volume. However, this method can present some limitations in the estimation of pore size for narrow mesopores ($\leq$ 10 nm), size will be underestimated in this case ~20-30%.[43].

2.3.3 Temperature Programmed Reduction (TPR)

Temperature programmed reduction (TPR) is one of the temperature programmed analysis techniques used for characterization of supported catalysts. In a TPR test, for mixed oxides, the catalyst is contained and heated under temperature programming in a

reducing environment, a mix stream containing H_2 (1%-10%) and an inert carrier gas (He, Ar or N_2) flows through the sample. H_2 will react with the mixed oxide. Afterwards, active metal and water will be produced affecting H_2 concentration in the carrier gas. Continuous monitoring of this effect is made by a thermal conductivity detector (TCD). Thus, it can provide valuable information about the number of reducible species in the catalyst and reveals the temperature at which the reduction occurs [44].

2.3.4 H_2 Chemisorption

Chemisorption can be defined as an adsorption type resultant from a chemical bonding formation between the adsorbate and the surface of the adsorbent. It can be used for characterizing the catalyst metallic surface area. Hydrogen will be dissociative adsorbed, meaning each gas atom will form a bond with one active site from the metal surface. Afterwards, the quantity of chemisorbed hydrogen can be measured and the number of active sites can be found [40].

With the sample adsorbed gas quantity or isotherm, graphical and numerical methods can be used to find the monolayer capacity, V_m. At least three points of the isotherm will be needed, pressure at this point should be in a region where the monolayer formation is assured, so points should be chosen from the low-slope section. Physisorption can be considered zero at zero pressure. Extrapolating this line back to zero pressure, V_m will be found as the intercept on the y-axis. This value represents all chemisorbed gas without chemisorption strength being considered. Applications that, as in this case, require for only strong chemisorption sites will need a second isotherm that represents only the weak sites. The difference between both isotherms will represent the strong chemisorption amount [40].

Using the Langmuir model number of metal atoms, metal area and dispersion can be calculated from equations 2.4 to 2.6.

$$N_a = \frac{V_m}{22414} LS \qquad (2.4)$$

$$A_w = \frac{N_a A_x}{W} \qquad (2.5)$$

$$\delta\,(\%) = \frac{N_a}{N_t} \times 100\% \qquad (2.6)$$

Where :N_a is the number of metal atoms ,V_m is the monolayer volume (ml) at standard pressure and temperature, L is the Avogadro's number (6.022×10^{23}), S is the adsorption stoichiometry (2 for H_2), A_w = Active metal area, A_x = surface atom cross sectional area, W= mass, δ (%) = exposed metal atoms (%) and N_t = total metal content.

2.3.5 Gas chromatography

Chromatography is a separation and analysis method where the divided components are disseminated in two phases: a stationary phase which could be liquid or solid with a large surface area, and a mobile phase (gas or liquid) that flows through the stationary bed [45].

Gas chromatography is the most popular technique for separation and analysis of volatile compounds. It can make simple, fast, reliable and highly accurate analysis over a large set of organic and inorganic materials.

Procedure can be described as follows. The sample enters a heated injection port where is vaporized and then carried by an inert gas (mobile phase) that flows continuously through the system. Flow rate must be constant to ensure a proper analysis, gas mixture then passes through the stationary phase (capillary columns), which can contain the gas and make the process leak free, then sample partition takes place. Here, components are separated based on solubility with the stationary bed and relative vapor pressures. Afterwards, sample in the carrier gas passes through a detector that measures the sample quantity producing an output signal. The system will analyze the data, generate a chromatogram and integrate the peak area, here system can also measure peak height, but given the computer advances the peak area is considered more reliable [45].

For a quantitative analysis there are several methods that can be employed, one of the most popular is the external standard. This procedure can be performed graphically or by a data system. The graphic method is more precise, it consists on chromatograph a known amount of the sample of interest generating a calibration curve that will be taken as the reference value against new samples will be compared [45].

3. EXPERIMENTAL

3.1 Material and equipment

Detailed chemicals and gases used for catalyst (synthesis, characterization) and DRM activity test are listed on table 3.1.

Table 3.1 Chemicals and gases used

Material	Formula	Molecular weight (g/mol)	Manufacturer	Purity %
Iron (III) Nitrate Nonahydrate	$Fe(NO_3)_3 \cdot 9H_2O$	403.95	EMSURE	≥ 99%
Nickel (II) Nitrate Hexahydrate	$Ni(NO_3)_2 \cdot 6H_2O$	290.81	EMSURE	≥ 99%
Aluminum Nitrate Nonahydrate	$Al(NO_3)_3 \cdot 9H_2O$	375.13	EMSURE	≥ 98.5%
Magnesium Nitrate Hexahydrate	$Mg(NO_3)_2 \cdot 6H_2O$	256.41	EMSURE	≥ 99%
Sodium Carbonate	Na_2CO_3	105.99	EMSURE	≥ 99.9%
Sodium Hydroxide	NaOH	40.00	AnalaR NORMAPUR	≥ 99.2%
Aluminum Oxide α phase	AL_2O_3	99	Sigma-Aldrich	≥ 99%
Carbon Dioxide	CO_2	44	Yara Praxair	≥ 99.999%
Methane	CH_4	16	Yara Praxair	≥ 99.999%
Helium	He	2	Yara Praxair	≥ 99.999%
Hydrogen	H_2	2	Yara Praxair	≥ 99.999%
Nitrogen	N_2	28	Yara Praxair	≥ 99.999%
Synthetic air	$N_2 + O_2$	28.9	Yara Praxair	≥ 99.999%

3.2 Catalyst synthesis

Four Catalyst batches were synthetized by coprecipitation at high supersaturation. Same conditions and concentrations were used for all batches and are given on table 3.2.

Table 3.2 Composition in reduced catalysts

Fe/Ni ratio	Composition in reduced catalyst (wt. %)				Preparation Method
	Ni	Fe	MgO	Al_2O_3	
0.1	20	2	52	26	Coprecipitation (high supersaturation)

Each of the four HT- like catalysts were prepared by coprecipitation at high supersaturation following a modified procedure based on the study presented by Tathod and Gazit [32] at a chosen Fe/Ni molar ratio x = 0.1. According to calculations presented on appendix, an stoichiometric measure of $Al(NO_3)_3 \cdot 9H_2O$, $Mg(NO_3)_2 \cdot 6H_2O$, $Fe(NO_3)_3 \cdot 9H_2O$ and $Ni(NO_3)_2 \cdot 6H_2O$ were mixed in 100 ml of deionized water with a 0.25 M metal nitrate concentration. A base solution of 500 ml containing Na_2CO_3 and NaOH was also prepared (pH=13), one equivalent of Na_2CO_3 was excessively added to ensure pillaring. Both solutions were kept on a magnetic stirrer for 15 minutes before final mixing. Nitrate solution was then swiftly added into the base solution using a syringe while on vigorous stirring. The mixed solutions were continued for 3 minutes. Afterwards the slurry solution was aged at 85 °C for 18 hours with vigorous stirring under continuous nitrogen purge. Aged solution was then filtered under vacuum condition, washing it with deionized water until a neutral pH could be measured on the filtrate, a 5-13µm filter was used in the process. Later the filter cake was dried on oven at 90 °C overnight. The dried solid was then crushed, sieved (0.15 µm size) and stored in a desiccator.

3.2.1 Calcination

The as- prepared catalyst precursors were calcined on a quartz reactor in flowing synthetic air, at three different temperatures of 500 °C, 600 °C and 700 °C with a temperature ramp rate of 5°C/min. The calcination process lasted 6 hours. After calcination calcined catalyst were re-crushed and sieved for having a more precise particle size range of 0.10- 0.15 µm. smaller particle size $\leq$ 0.1 µm were utilized for catalyst characterization tests. Notation and graphic representation for calcined samples in this study is presented on table 3.3.

Table 3.3 Calcined samples notation

Calcination Temperature	Notation	Notation Color
500 °C	C-500	Orange
600 °C	C-600	Blue
700 °C	C-700	Green

3.2.2 Reduction

Calcined catalysts were reduced prior to activity test in a fixed tubular reactor under a H_2/N_2 mixture with 1:1 ratio at a 100 mL/min flow rate for 4 hours. At different temperatures of 500 °C, 600 °C and 700 °C with a ramp rate of 5 °C/min for different DRM reactions tests. Notation for reduced samples included R- followed by its reduction temperature.

3.3 Catalyst characterization

3.3.1 X-Ray Diffraction (XRD)

XRD analysis of the as-prepared and calcined catalysts was made on Bruker-AXS Microdiffractomer D8 Advance with Cu*K*α as radiation source. A step interval of 1 °/min and a 2θ range of 10-90° were used for pattern recording.

3.3.2 N_2 adsorption-desorption

Approximately 120 mg each of as- prepared and calcined catalyst were degassed at 150°C overnight under vacuum condition. Tests were made on a Micromeritics Tristar 3000 instrument using liquid nitrogen at -196 °C.

3.3.3 Temperature Programmed Reduction (TPR)

Approximately 100 mg of each calcined catalyst were tested on The Micromeritics Autochem II ASAP 2920 analyzer for H_2-TPR measurements. After setting cold trap (~ -18 °C) and starting the program, samples were degassed for removing adsorbed H_2O and CO_2 with Helium flow during 30 minutes at 200 °C. After cooling samples to 50 °C TPR analysis begins by flowing the reducing gas mixture (10% H_2, 90% Ar) through the sample at a 50 mL/min flowrate. While the gas is flowing temperature of the sample is increased linearly to 950 °C with a ramp up rate of 10 °C/ min and kept for 30 minutes.

3.3.4 Hydrogen chemisorption

This characterization test was made after all DRM activity tests were finished, based on results only the sample calcined at 600 °C was used. The analysis was carried out on a

Micromeritics ASAP 2020 Plus instrument.~ 200 mg of C600 samples were degassed at 200 °C (ramped up at 5°C/min) for 2 hours, reduced in flowing hydrogen at 500 °C , 600°C and 700 °C for 4 hours (ramped up at 5 °C/min). Then cooled down by flowing nitrogen. Ultimately hydrogen chemisorption analysis occurred at 35 °C.

3.4 DRM activity test

DRM reaction was carried on a fixed-bed tubular reactor made of a special metal alloy with high temperature resistance. During test, temperature was controlled by a Eurotherm 3280 regulator that was connected to the electrical oven of the system. Reactor had an inner diameter of 11.81 mm and a thermocouple (type K) was installed above the catalyst bed. The rest of the system consisted on gas cylinders (N_2, H_2, CH_4 and CO_2) connected to lines that went to the reactor system. The gas flow was controlled by mass flow controllers (Alicat gas mixer), manual valve regulators were installed to control gas pressure entering the system. Pressure in the reactor can be seen on an installed pressure gauge.

In a typical testing experiment, 50 mg of calcined catalyst (0.10 μm -0.15μm) were mixed with 500 mg of α-alumina (100-200 mesh) for improving contact area and heat transfer. Quartz wool was placed inside the reactor and catalyst were poured on top of it. Reactor was checked to ensure the catalyst not to be lost or out of position during the experiment. After setting the montage mixer was turned on a gas mixture flow (50/50 vol%) of H_2 and N_2. Then, 100 mL/min were purged in the reactor with temperature at a ramp up rate of 5°C/min. Temperature increase continued until target reduction temperature was achieved, 3 different reduction temperatures were tested for each of the calcined samples as stated on table 3.4. Afterwards a flow 100% N_2 at 200 mL/min was purged into the reactor for 1 hour. N_2 ramped up temperature to reaction temperature of 700°C at a 5°C/min if necessary. Finally, reactant gases mixture (50/50 vol%) CH_4 and CO_2 started flowing through reactor at 100 mL/min (120,000 $mL/g^{-1}{\cdot}h^{-1}$ of GHSV) and pressure of 1 bar. All gases were preheated before their reactor entrance by passing through a line in the oven.

Off-gas mixture goes to the gas chromatograph (Agilent 7890B) for online analysis. Before getting to the GC the gas mixture current must be split and vent part of it to ensure a smaller and more stable flow. Moreover, liquid was also not allowed in GC, so off-gas passed through a coalescing water filter. Reaction products (CH_4, CO_2, H_2 and CO) were

then carried by a He and Ar stream on the GC where it was analyzed in a molecular sieve-packed column with two TCD detectors.

Results from GC were normalized. A carbon balance was performed, then reactant conversion and H_2/CO ratio calculations were made by molar balance, Equations 3.1 to 3.3.

$$X_{CH4} = \frac{n_{CH4}^{in} - n_{CH4}^{out}}{n_{CH4}^{in}} \times 100\% \qquad (3.1)$$

$$X_{CO2} = \frac{n_{CO2}^{in} - n_{CO2}^{out}}{n_{CO2}^{in}} \times 100\% \qquad (3.2)$$

$$\frac{H_2}{CO} = \frac{n_{H2}}{n_{CO}} \qquad (3.3)$$

4. RESULTS AND DISCUSSION

4.1 Characterization

4.1.1 XRD analysis

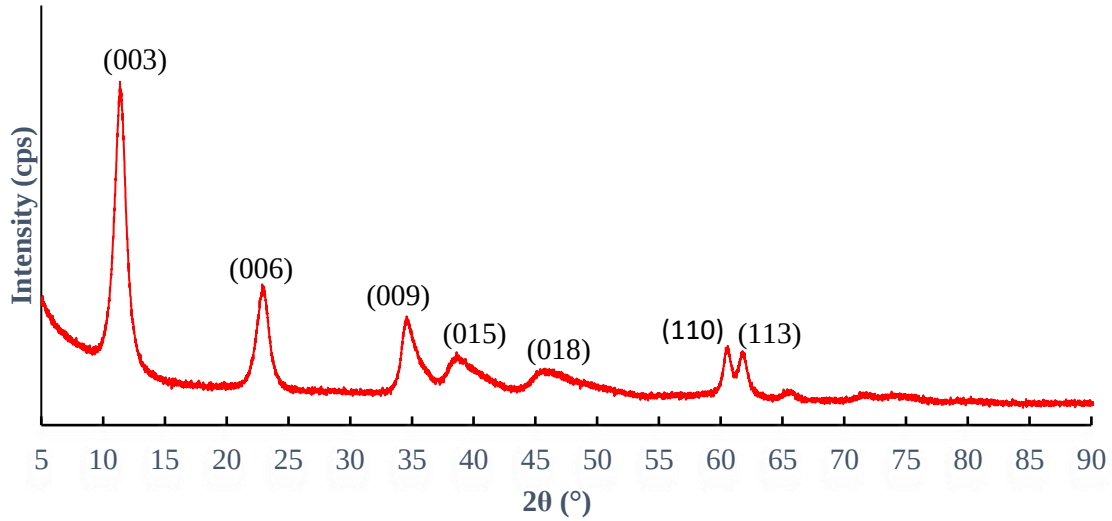

Figure 4.1 As-prepared catalyst XRD synthesized by coprecipitation at high supersaturation

As- prepared catalyst XRD profile from figure 4.1 shows four sharp and symmetrical diffraction peaks at 2θ = 11.37°, 22.88° , 60.56° and 61.76°, which are attributed to (003), (006), (110), (113) planes, and three broad diffraction peaks at 2θ = 34.57°, 38.61°, and 45.79°, which correspond to (009), (015) and (018) planes, respectively. These results are consistent with diffraction peaks from magnesium aluminum hydroxide carbonate HT (JCPDS 22-0700). The as-prepared catalyst was confirmed to be well prepared with high purity and crystallinity by this rapid coprecipitation method. The precursors were successfully washed, no impurities such as potassium salt were found [33, 46].

d-spacing from (003) diffraction peak was used for calculating the thickness between one interlayer and a brucite-like sheet. The result, 0.778 nm, was a slightly smaller than 0.784 nm of magnesium aluminum hydroxide carbonate HT. d- spacing from (110) was used for calculating the average cation-cation distance in the brucite-like layer, which is two times d (110) [12, 46]. As for the as-prepared precursors, d (110) was 0.153 nm which is a slightly smaller than the reference value (0.154 nm) of magnesium aluminum hydroxide carbonate. It can be due to the substitution of the Mg^{2+} ion (0.072 nm) to the smaller Ni^{2+} (0.069 nm) that brucite layer thickness was reduced.

.

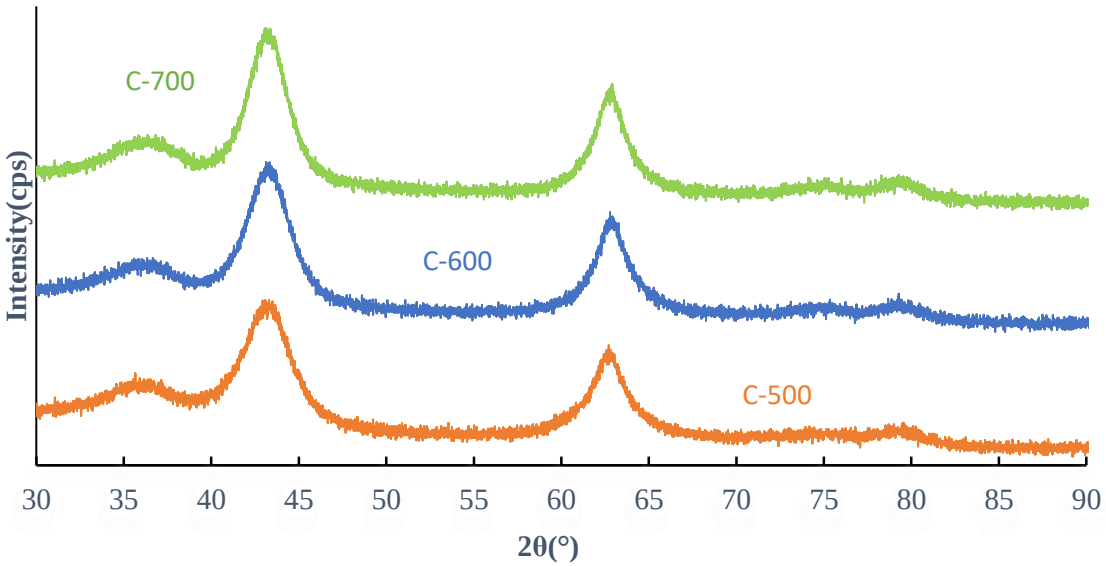

Figure 4.2 XRD of calcined catalysts (at different calcination temperature 500 °C, 600°C and 700 °C)

The precursors were calcined at three different temperatures of 500 °C, 600 °C and 700°C for 6 hours. From XRD analysis it can be conclude that the precursors were successfully decomposed from hydroxide state to oxide state under these calcination conditions, as none of the characteristic diffraction peaks of HT material were observed. Diffraction peaks data of calcined catalysts are displayed on table 4.1 and could be attributed to diffraction of NiO (JCDPS 01-089-5881) but could also be assigned to $MgAl_2O_4$, $NiFe_2O_4$, $NiAL_2O_4$ and Fe_2O_3 because of possibly overlapping peaks.

Table 4.1 Diffraction peaks data and crystallite size of calcined samples.

Sample	Peak 1	Peak 2	Peak 3	Peak 4	Peak 5	Crystallite size (nm)
C-500	35.65°	43.29°	62.71°	74.16°	79.54°	3.08
C-600	36.32°	43.14°	62.78°	75.35°	79.28°	3.57
C-700	36.37°	43.09°	62.9°	74.12°	79.28°	3.88

Higher peak intensity with temperature increase is observed from figure 4.2. A close up of peak 2 is presented in figure 4.3. In fact, based on Scherrer's equation, the crystallite size was calculated as shown in table 4.1. It shows that for higher calcination temperature, the oxide crystallite size increases.

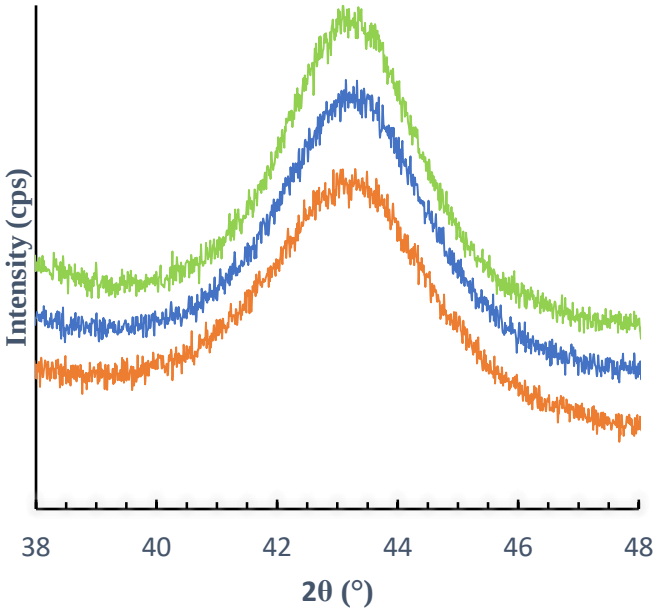

Figure 4.3 XRD calcined peaks used to calculate crystallite size Scherrer equation

4.1.2 N_2 Adsorption-desorption

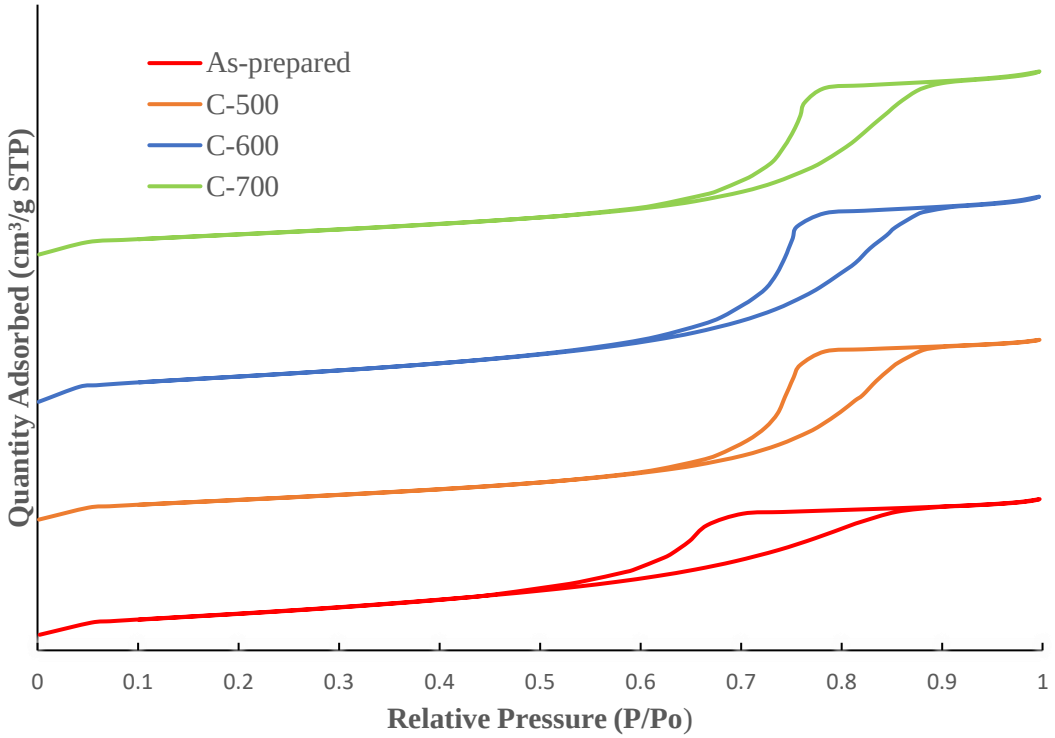

Figure 4.4 N2 Adsorption-Desorption isotherms for as-prepared and calcined catalysts

After thermal decomposition, structural changes are expected for the as-prepared sample. A direct comparation by N_2 adsorption isotherms for as-prepared and calcined catalysts is shown in figure 4.4.

According to IUPAC classification, the isotherms of calcined catalysts with hysteresis in high pressure zone could be assigned to as type IV isotherm , which is representative for mesoporous material [42].

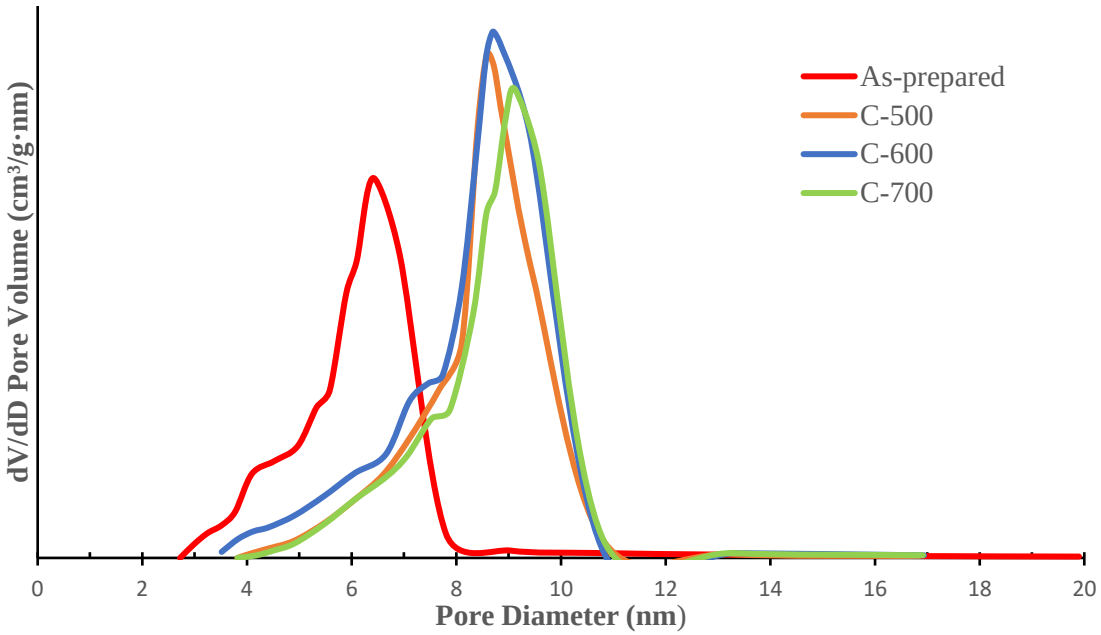

Figure 4.5 Pore size distribution of as prepared and calcined catalysts

Moreover, narrow pore size distribution was observed in the as-prepared and calcined catalysts, as shown in figure 4.5. Thermal decomposition increased the average pore size of calcined catalyst from 5-7 nm to 8-10 nm. This size ranges also are in good agreement with IUPAC classification of mesoporous material with pores of widths between 2nm and 50 nm.

Table 4.2 Textural properties of as-prepared and calcined catalysts

Sample	BET Specific surface Area (m^2/g)	BJH Pore Volume (cm^3/g)
As-prepared	229.47	0.45
C-500	202.08	0.57
C-600	239.59	0.63
C-700	209.14	0.56

Textural properties for all samples are summarized in table 4.2. High surface area (more than 200 m^2/g) and pore volume was found for the as-prepared HT-like material and calcined catalysts. The effect of calcination temperature on the textural properties is significant. Pore volume increased due to water and other gaseous products from decomposition were released from the gallery between brucite-like layers and the LDH collapsed structure. Hence, more channels were created and the porosity of the catalysts was enhanced [12]. On the other hand, the changes in surface area showed a different behavior. As for C-700 catalyst, the decrease in surface area could be due to a too high calcination temperature. According to Fornasari *et al.* [47] surface area could decrease significantly for Ni/MgAl catalysts with the increase of calcination temperature. Likewise, for catalyst calcined at 500 °C, a reduce in surface area is also observed, which is assumedly because of incomplete decomposition of the layer structure. In contrast, the catalyst C-600 had the higher surface area after calcination compared to the as-prepared precursors. It is suggested that 600 °C is the most suitable calcination temperature, where extra porosity and channels were created generating an increase in surface area and pore volume.

4.1.3 TPR

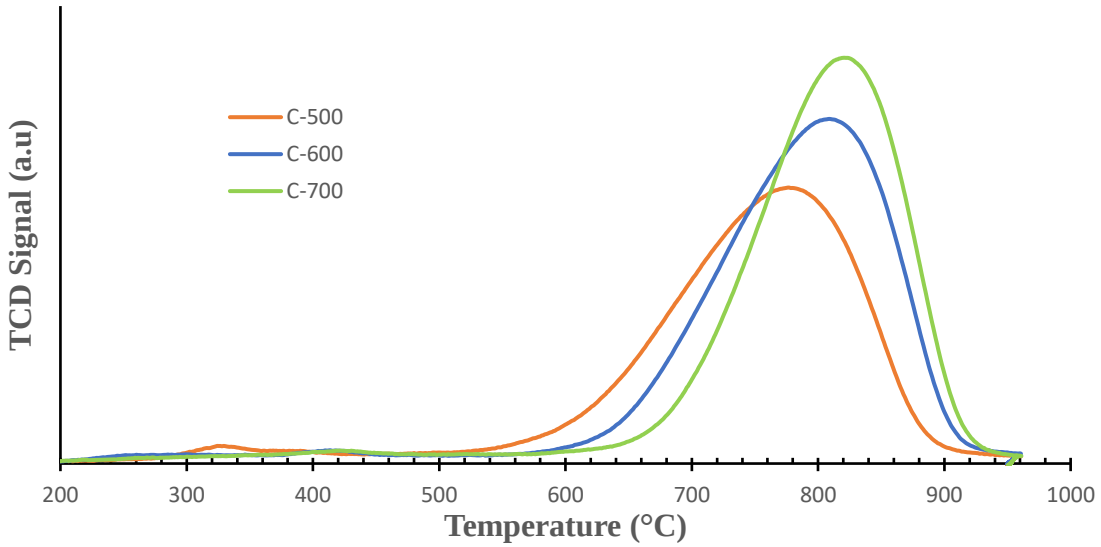

Figure 4.6 TPR patterns of calcined catalyst

TPR tests were conducted for analyzing the calcined catalysts reduction performance. Graphical representation is found on figure 4.6 and summarized results are given on table 4.3. The degree of metal-support interaction can be determined according to TPR peak

temperature, a shift to higher temperature is evidence of a stronger metal-support interaction.

There is an optimum level for this interaction to happen, if is too weak catalyst will be quickly deactivated by sintering or carbon deposition, and if is too strong not enough active sites will be free for having a high conversion on DRM reaction. Choosing the optimal interaction level is a compromise between stability and activity [48]. It can be appreciated that with the increasing calcination temperature, reducibility will decrease, these results are in accordance with studies on Ni species by Cavani *et al.* and Tichit *et al.* [12, 49]

For each TPR profile, two peaks can be noticed, the small peak can be assigned to surface reduction from Fe^{3+} to Fe^{2+}. This peak has a considerable temperature difference between C-500 (324 °C) and C-600 (414 °C), C-700 (421 °C). Main peaks can be associated to the coreduction of Ni^{+2} to Ni^{0} as well bulk Fe^{+3} and surface Fe^{+2} to Fe^{0} [50].

Table 4.3 TPR peak temperatures and H2 chemisorbed for calcined catalysts

Temperature Programmed Reduction Results		
Sample	Peak Temperature	H_2 Consumption (µmol/g)
C 500	777 °C	2.97
C 600	808 °C	3.17
C 700	821 °C	3.24

4.1.4 Chemisorption

H_2 Chemisorption tests were realized for C-600 sample, results are summarized in table 4.1. It is assumed that H_2 is only being chemisorbed on metallic Ni for a simplified analysis.

Table 4.4 C-600 chemisorption tests at different reduction temperatures

Sample	H2 chemisorption (µmol/g)	Ni Dispersion (%)	Metallic surface area (m2/g)
C-600 R-500	4.656	0.27%	0.36
C-600 R-600	54.188	3.18%	4.23
C-600 R-700	75.001	4.40%	5.86

All the analyzed parameters for C-600 increased with reduction temperature. This behavior is in accordance with results from Alzamora *et al* [51]. The biggest change was from R-500 to R-600 where H_2 chemisorption, Ni dispersion and metallic surface area increased by a factor of 11.7.

4.2 DRM activity

A test matrix was planned for realizing activity tests for different calcination and reduction temperatures, each of the calcined samples were reduced at three different reduction temperatures (500 °C, 600° C, 700 °C) previous to activity test. Thus 9 different conditions were tested for DRM reaction. Reaction temperature (700 °C) and reactants gas hourly space velocity GSHV (120,000 $mL/g^{-1}\cdot h^{-1}$) were kept constant. For interpretation purposes results will be presented by calcination temperatures.

4.2.1 DRM activity for catalyst calcined at 500°C

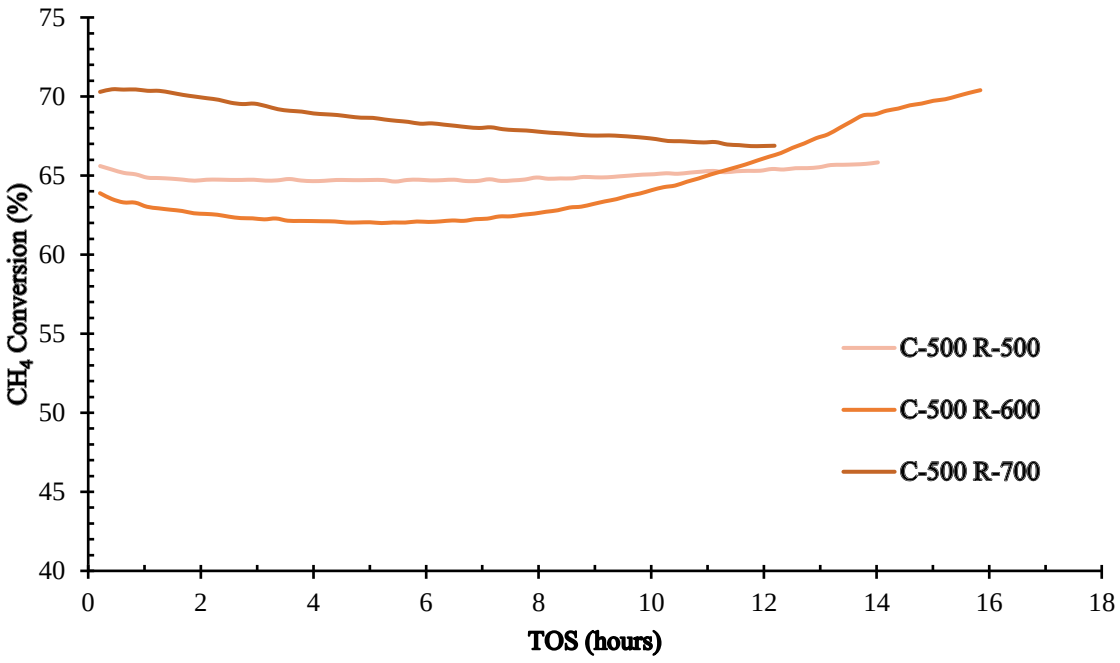

Figure 4.7 CH4 conversion of samples calcined at 500°C at different reduction temperatures

All samples presented different behaviors during reaction proving the effects of reduction temperature over a calcined catalyst. Figure 4.7 showed the CH_4 conversion of C-500 in DRM reaction at different reduction temperature. R-700 started at 70.5 % (maximum conversion) which can be due to a complete reduction at 700°C of the catalyst prior to reaction. However, the conversion was steadily declining during reaction. It is suspected that sintering occurred at the surface area of big sized particle. C500 had the lower TPR

peak, afterwards sintering deactivation over big particle size could started to happen. R-600 follows a different trend, conversion started at 63.9% declining slowly for almost 6 hours, then the conversion steadily increased for the next 10 hours of time on stream (TOS), reaching 70.4% and showing no signs of deactivation. R500's conversion declined 1% in the first 2 hours; however, the conversion slowly increased and recovered its initial maximum conversion.

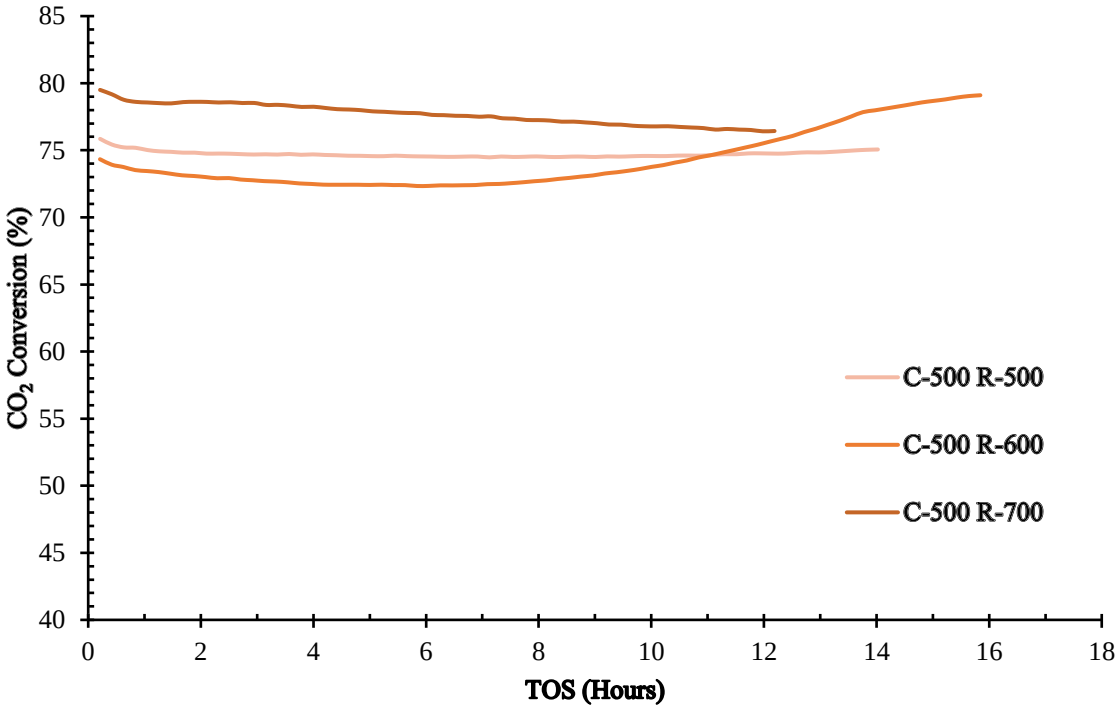

Figure 4.8 CO2 conversion for samples calcined at 500°C at different reduction temperatures

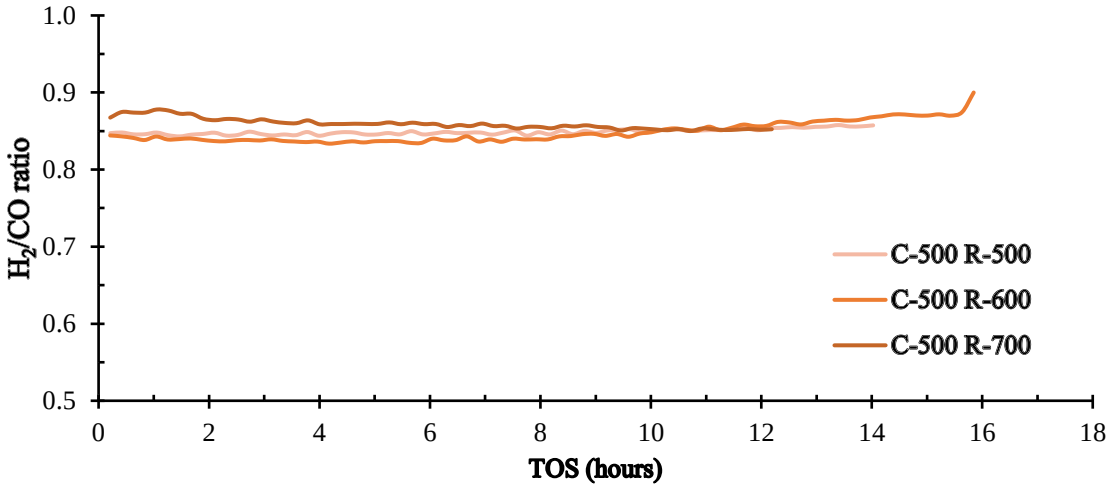

Figure 4.9 H2/CO ratio for samples calcined at 500°C at different reduction temperatures

CO_2 production from figure 4.8 follows same tendencies as CH_4, although the conversions were higher than CH_4 conversions due to the effect of RWGS. This side reaction consumed H_2 and CO_2 to produce CO and water, which is why H_2/CO ratio was below 1, as shown in figure 4.9.

4.2.2 DRM activity for catalyst calcined at 700°C

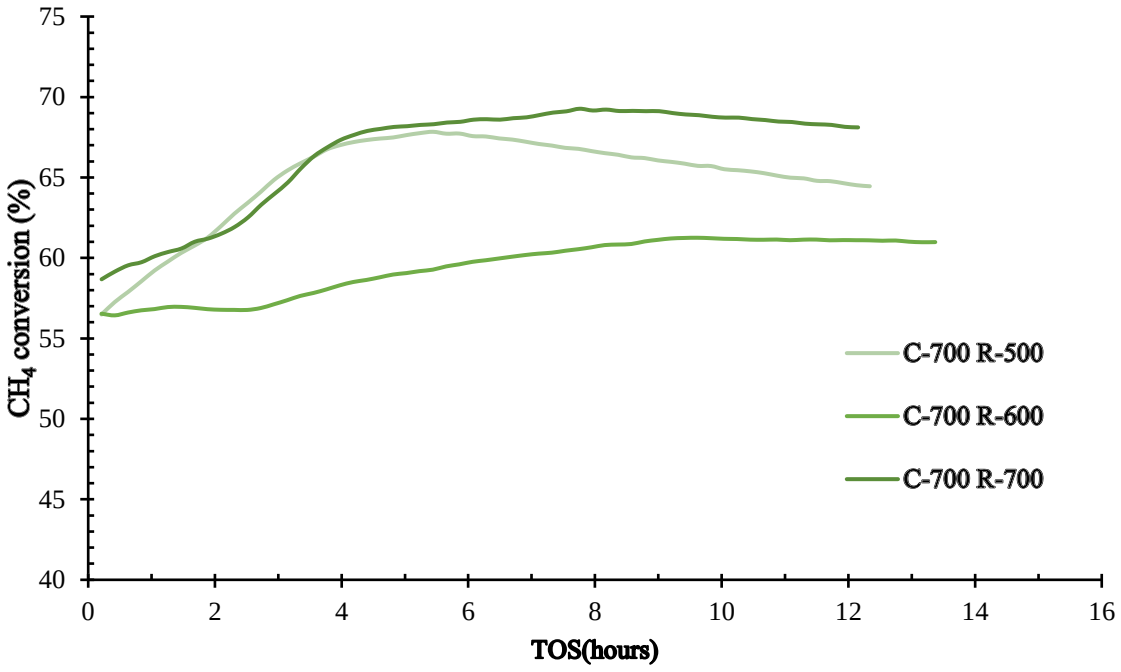

Figure 4.10 CH4 conversion for samples calcined at 700°C at different reduction temperatures

CH_4 conversion of C-700 catalysts in DRM reaction at different reduction temperatures is presented in figure 4.10. C-700 possessed the highest reduction peak among the studied catalysts, corresponding to strong metal-support interaction. Hence, it is assumed that C-700 was difficult to be reduced and the reduction could be occurred during reaction where H_2 as a product existed. As a result, an increase in conversion during activity test is predicted, R-700 exhibited significant increase in conversion from 58.3% to 69.3%, during the first 8 hours of TOS. Likewise, R-600 also increased in conversion but less remarkably than R-700. 61.3% of CH_4 had been stably converted after 9 hours of TOS. The catalyst in this condition performed good stability with minimal deactivation. As for R-500, a rapid increase in conversion was also observed but followed by a significant drop after 5 hours of TOS.

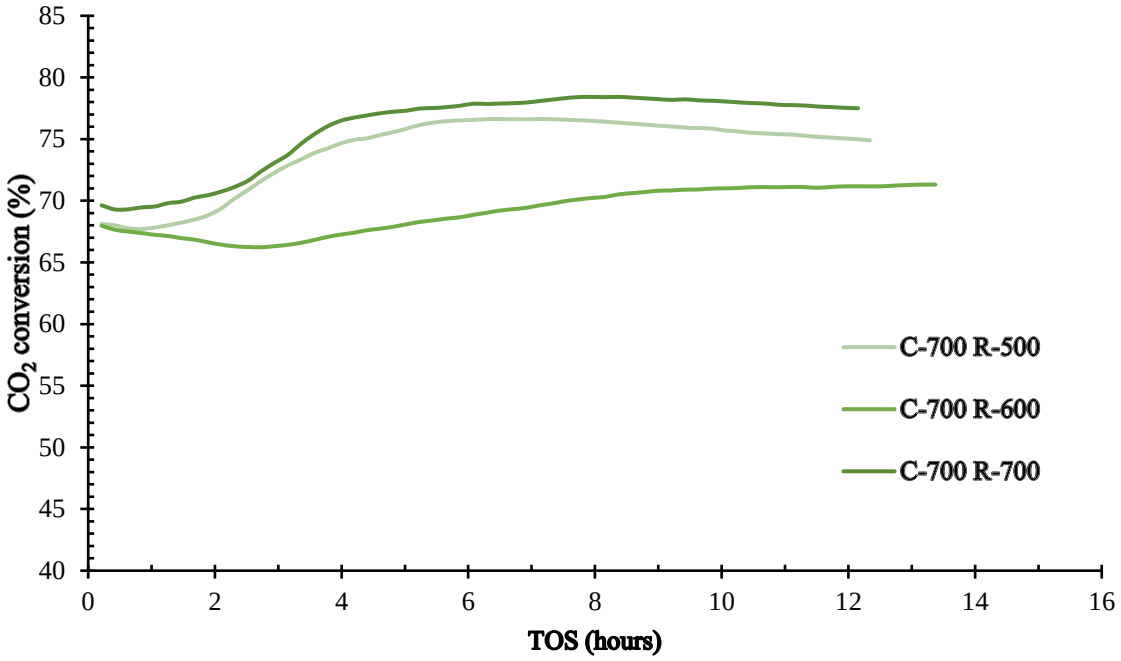

Figure 4.11 CO2 conversion for samples calcined at 700°C at different reduction temperatures

CO_2 conversion from figure 4.11 follows same tendencies as CH_4 for R-600 and R-700, Although the CH_4 conversion of R-500 experienced a sudden drop after 5 hours of TOS, CO_2 conversion was slightly decreased by only 2%. This can be explained by the side reaction RWGS which kept consuming CO_2 and maintaining H_2/CO ratio, as showed in figure 4.12. The CO_2 conversion of R-600 declined not as rapid as in CH_4.

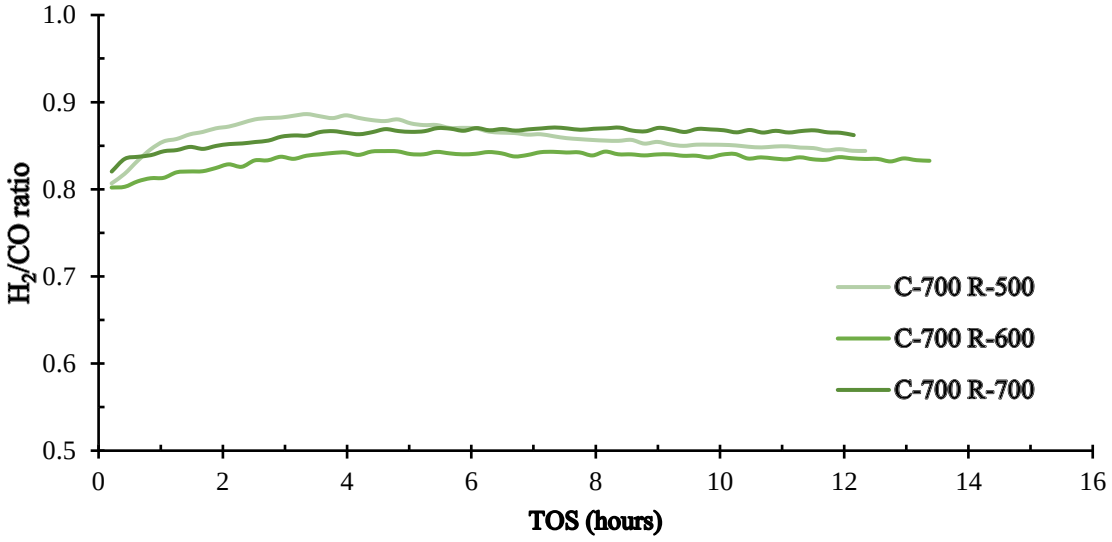

Figure 4.12 H2/CO ratio for samples calcined at 700°C at different reduction temperatures

4.2.3 DRM activity for catalyst calcined at 600°C

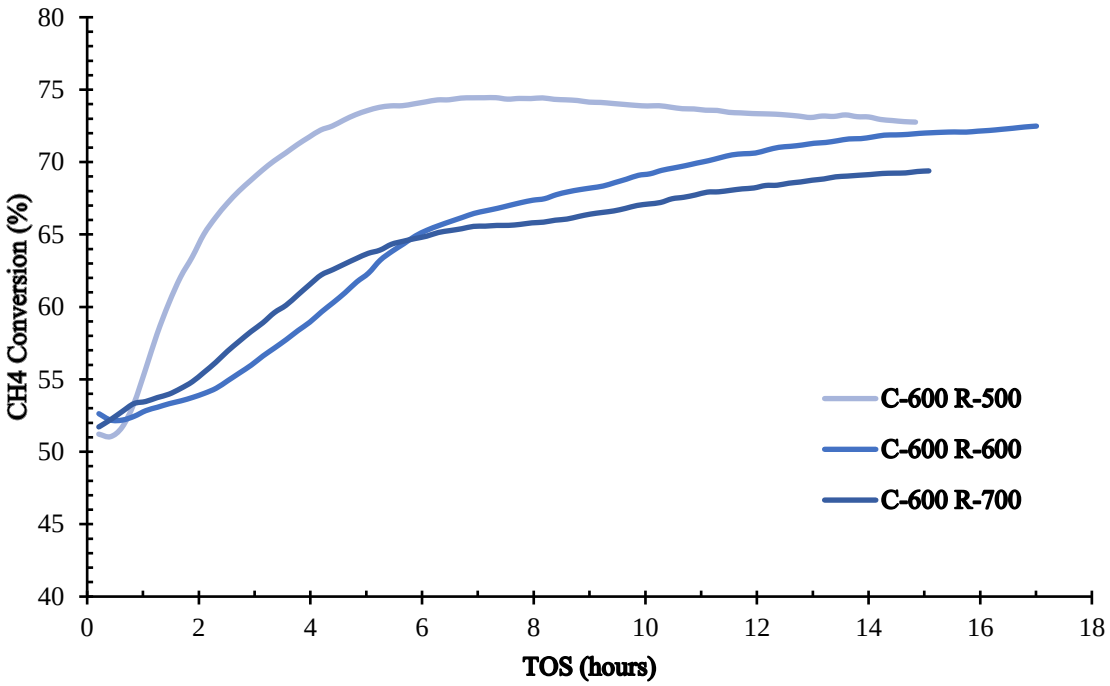

Figure 4.13 CH4 conversion for samples calcined at 600°C at different reduction temperatures

CH_4 conversions for calcined samples at 600 °C are presented in figure 4.13. All C-600 samples started with low conversion values around 51% to 53% followed by a rapid increase. It is supposed that its high reduction temperature makes catalysts not completely active at start of reaction. In fact, it has been confirmed by metal surface area data that R-700 sample had relatively more active sites than the other samples. R-600 and R-700 show no sign of deactivation after an average of 20% conversion increase and 15 hours TOS reaching conversions of 69.4% and 72.5% respectively. On the other hand, and despite having the highest conversion at 74.4%, R-500 was the only C-600 sample to show signs of deactivation after 8 hours of TOS. Rapid reduction during reaction could lead this sample to an early deactivation phase.

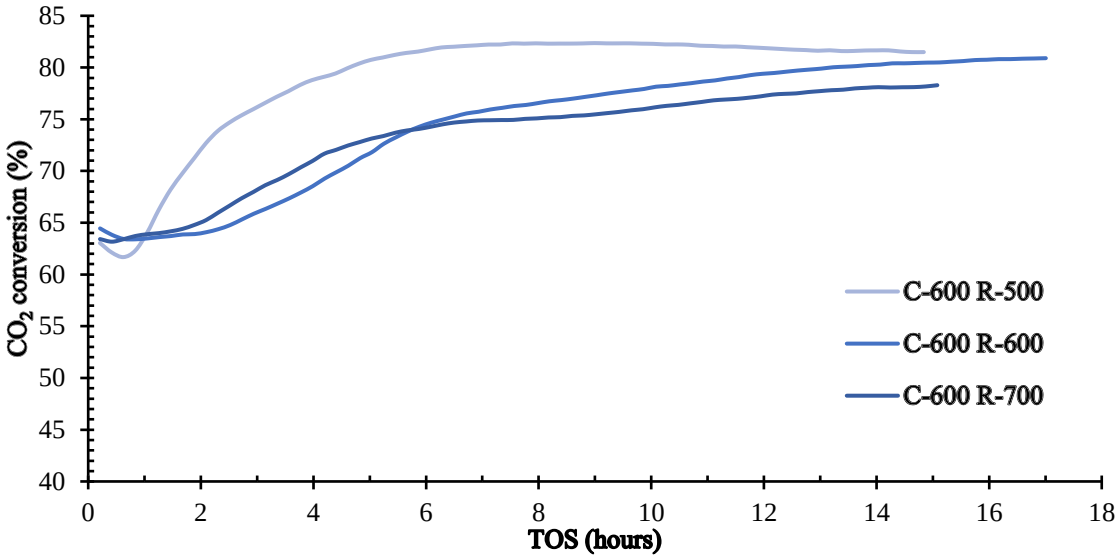

Figure 4.14 CO2 conversion for samples calcined at 600°C at different reduction temperatures

CO_2 conversion, as presented in figure 4.14, had a similar behavior with respect to CH_4 conversion as the ones at different calcination temperatures

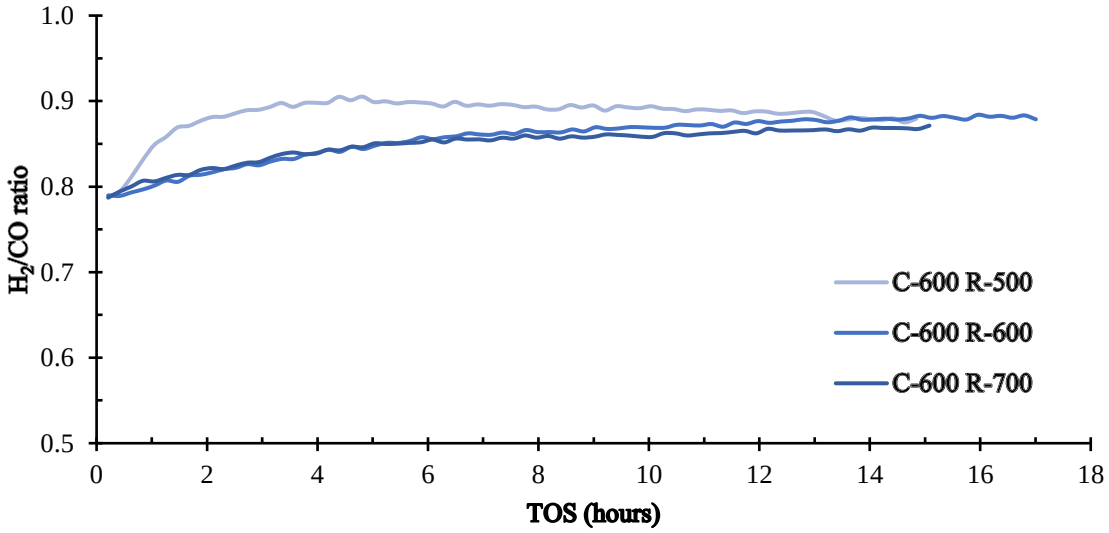

Figure 4.15 H2/CO ratio for samples calcined at 500°C at different reduction temperatures

C-600 sample was chosen for more testing, for having the best overall conversion and trends at all given reduction tests. This can be due to its superior surface area that is believed to be supported on an optimal particle size given by the right amount of LDH decomposition after calcination.

5. CONCLUSIONS AND RECOMMENDATIONS

5.1 Conclusions

Various bimetallic NiFe catalysts with $MgAl_2O_4$ support were successfully synthetized by coprecipitation at high supersaturation method with a constant Fe/Ni ratio of 0.1 and a Ni 20 wt%. From characterization of the calcined catalysts (500 °C, 600 °C, 700 °C). It can be concluded that:

- The HT precursors were successfully decomposed into mixed oxides at different calcination temperatures from 500 °C to 700 °C. No impurities were detected from XRD data and the crystallite size increased with temperature.
- Based on Bet results calcination temperature had a direct effect on surface area. High (700 °C) and low (500°C) temperatures had a detrimental effect for catalyst surface are compared with the as-prepared catalyst. On the other hand, sample calcined at 600 °C presented an increase in its surface area.
- Increase in calcination temperature generated an increase in pore volume and pore size. Besides, narrow pore size distribution was achieved due to the coprecipitation at high supersaturation method.
- Higher reduction peaks were observed with the calcination temperature increase.
- Ni dispersion and active metal area were affected of the calcined catalyst (600 °C) increased with reduction temperature (500 ° C to 700 °C). Very small values were presented for the 500 °C reduction.

Additionally, the impact of calcination and reduction temperatures on activity and stability for DRM conversion at 700°C. with a gas hourly space velocity (GHSV) of 120,000 $mL.g^{-1}.h^{-1}$ at atmospheric pressure was tested.

After the nine activity test were performed. It can be concluded that catalyst calcined at 600 °C presented the overall better performance for all reduction temperatures (500 °C, 600 °C and 700 °C). It achieved a CH_4 conversion of 72.5% with a 600°C reduction temperature. C-600 samples presented no sign of deactivation after 15 hours of TOS for 600°C and 700 °C reductions. This result can be due to C-600 having the highest surface area from the study, and what could be an ideal metal-support interaction strength when compared with the other calcined samples.

Catalyst calcined at 700 °C presented the lower conversions at all reduction temperatures, when compared with the other calcined catalyst. This result suggest that calcination temperature have a bigger effect over activity than the reduction temperature.

Despite its lower peak conversion values when compared with 600 °C catalyst, The C-500 presented interesting results in stability, with an almost constant CH_4 conversion of 65.8% for the test reduced at 500°C. deactivation signs where only present for reduction at 700 °C test.

For all calcined samples CO_2 conversion was higher than CH_4 conversion due to the effect of the RWGS reaction. Besides, it was less prone to deactivation than CH_4 conversion.

5.2 Recommendations

- Additional studies can be made with a suggested calcination and reduction temperatures between 500 °C and 600 °C, it is possible that optimum temperature for this specific catalyst is in that range.
- For catalyst conditions that showed no sign of deactivation, run activity test at a higher proposed temperature of 800 °C to obtain better conversions. Then, check if stability is maintained.
- Increase the catalyst molarity from 0.25 M, for synthetizing more catalyst. At the moment, catalyst produced is not enough for realizing all possible test with various repeatability runs
- Provide maintenance to laboratory equipment's on months previous to master thesis experiments.

REFERENCES

[1] S.-E. Park, J.-S. Chang, and K.-W. Lee, *Carbon Dioxide Utilization for Global Sustainability: Proceedings of the 7th International Conference on Carbon Dioxide Utilization, Seoul, Korea, October 12-16, 2003*. Elsevier, 2004.

[2] P. Markewitz *et al.*, "Worldwide innovations in the development of carbon capture technologies and the utilization of CO2," *Energy & Environmental Science*, 10.1039/C2EE03403D vol. 5, no. 6, pp. 7281-7305, 2012, doi: 10.1039/C2EE03403D.

[3] N. A. K. Aramouni, J. G. Touma, B. A. Tarboush, J. Zeaiter, and M. N. Ahmad, "Catalyst design for dry reforming of methane: analysis review," *Renewable and Sustainable Energy Reviews*, vol. 82, pp. 2570-2585, 2018.

[4] B. Nematollahi, M. Rezaei, and M. Khajenoori, "Combined dry reforming and partial oxidation of methane to synthesis gas on noble metal catalysts," *International journal of hydrogen energy*, vol. 36, no. 4, pp. 2969-2978, 2011.

[5] B. Abdullah, N. A. A. Ghani, and D.-V. N. Vo, "Recent advances in dry reforming of methane over Ni-based catalysts," *Journal of Cleaner Production*, vol. 162, pp. 170-185, 2017.

[6] J. Guo, H. Lou, H. Zhao, D. Chai, and X. Zheng, "Dry reforming of methane over nickel catalysts supported on magnesium aluminate spinels," *Applied Catalysis A: General*, vol. 273, no. 1-2, pp. 75-82, 2004.

[7] R. Dębek, M. Motak, T. Grzybek, M. Galvez, and P. Da Costa, "A short review on the catalytic activity of hydrotalcite-derived materials for dry reforming of methane," *Catalysts*, vol. 7, no. 1, p. 32, 2017.

[8] J.-E. Min, Y.-J. Lee, H.-G. Park, C. Zhang, and K.-W. Jun, "Carbon dioxide reforming of methane on Ni–MgO–Al2O3 catalysts prepared by sol–gel method: Effects of Mg/Al ratios," *Journal of Industrial and Engineering Chemistry*, vol. 26, pp. 375-383, 2015.

[9] Z. Bian, S. Das, M. H. Wai, P. Hongmanorom, and S. Kawi, "A review on bimetallic nickel-based catalysts for CO2 reforming of methane," *ChemPhysChem*, vol. 18, no. 22, pp. 3117-3134, 2017.

[10] H. Wu *et al.*, "Bi-and trimetallic Ni catalysts over Al2O3 and Al2O3-MOx (M= Ce or Mg) oxides for methane dry reforming: Au and Pt additive effects," *Applied Catalysis B: Environmental*, vol. 156, pp. 350-361, 2014.

[11] S. A. Theofanidis, V. V. Galvita, H. Poelman, and G. B. Marin, "Enhanced carbon-resistant dry reforming Fe-Ni catalyst: Role of Fe," *Acs Catalysis,* vol. 5, no. 5, pp. 3028-3039, 2015.

[12] F. Cavani, F. Trifiro, and A. Vaccari, "Hydrotalcite-type anionic clays: Preparation, properties and applications," *Catalysis today,* vol. 11, no. 2, pp. 173-301, 1991.

[13] P. Cao, S. Adegbite, H. Zhao, E. Lester, and T. Wu, "Tuning dry reforming of methane for FT syntheses: A thermodynamic approach," *Applied Energy,* vol. 227, pp. 190-197, 2018.

[14] M. K. Nikoo and N. Amin, "Thermodynamic analysis of carbon dioxide reforming of methane in view of solid carbon formation," *Fuel Processing Technology,* vol. 92, no. 3, pp. 678-691, 2011.

[15] S. T. Oyama, P. Hacarlioglu, Y. Gu, and D. Lee, "Dry reforming of methane has no future for hydrogen production: Comparison with steam reforming at high pressure in standard and membrane reactors," *International journal of hydrogen energy,* vol. 37, no. 13, pp. 10444-10450, 2012.

[16] M. Usman, W. W. Daud, and H. F. Abbas, "Dry reforming of methane: Influence of process parameters—A review," *Renewable and Sustainable Energy Reviews,* vol. 45, pp. 710-744, 2015.

[17] A. Ashcroft, A. K. Cheetham, M. Green, and P. Vernon, "Partial oxidation of methane to synthesis gas using carbon dioxide," *Nature,* vol. 352, no. 6332, p. 225, 1991.

[18] J. Rostrup-Nielsen and D. L. Trimm, "Mechanisms of carbon formation on nickel-containing catalysts," *Journal of Catalysis,* vol. 48, no. 1-3, pp. 155-165, 1977.

[19] M. Argyle and C. Bartholomew, "Heterogeneous catalyst deactivation and regeneration: a review," *Catalysts,* vol. 5, no. 1, pp. 145-269, 2015.

[20] J.-H. Kim, D. J. Suh, T.-J. Park, and K.-L. Kim, "Effect of metal particle size on coking during CO2 reforming of CH4 over Ni–alumina aerogel catalysts," *Applied Catalysis A: General,* vol. 197, no. 2, pp. 191-200, 2000.

[21] R. Martınez, E. Romero, C. Guimon, and R. Bilbao, "CO2 reforming of methane over coprecipitated Ni–Al catalysts modified with lanthanum," *Applied Catalysis A: General,* vol. 274, no. 1-2, pp. 139-149, 2004.

[22] P. Frontera, A. Macario, A. Aloise, P. Antonucci, G. Giordano, and J. Nagy, "Effect of support surface on methane dry-reforming catalyst preparation," *Catalysis today*, vol. 218, pp. 18-29, 2013.

[23] J. Ashok and S. Kawi, "Steam reforming of toluene as a biomass tar model compound over CeO2 promoted Ni/CaO–Al2O3 catalytic systems," *International journal of hydrogen energy*, vol. 38, no. 32, pp. 13938-13949, 2013.

[24] "Mineral Commodity Summaries 2019," in "Mineral Commodity Summaries," Reston, VA, Report 2019. [Online]. Available: http://pubs.er.usgs.gov/publication/70202434

[25] V. Galvita, T. Schröder, B. Munder, and K. Sundmacher, "Production of hydrogen with low COx-content for PEM fuel cells by cyclic water gas shift reactor," *International Journal of Hydrogen Energy*, vol. 33, no. 4, pp. 1354-1360, 2008.

[26] C. Forano, U. Costantino, V. Prévot, and C. T. Gueho, "Layered double hydroxides (LDH)," in *Developments in clay science*, vol. 5: Elsevier, 2013, pp. 745-782.

[27] S. M. Auerbach, K. A. Carrado, and P. K. Dutta, *Handbook of layered materials*. CRC press, 2004.

[28] A. V. Rane, K. Kanny, V. Abitha, and S. Thomas, "Methods for Synthesis of Nanoparticles and Fabrication of Nanocomposites," in *Synthesis of Inorganic Nanomaterials*: Elsevier, 2018, pp. 121-139.

[29] A. Bhattacharyya, "Method of hydrocarbon reforming and catalyst precursor," ed: Google Patents, 2000.

[30] A. P. Tathod and O. M. Gazit, "Fundamental insights into the nucleation and growth of Mg–Al layered double hydroxides nanoparticles at low temperature," *Crystal Growth & Design*, vol. 16, no. 12, pp. 6709-6713, 2016.

[31] J. Nyvlt, O. Sohnel, M. Matuchova, and M. Broul, "The kinetics of industrial crystallization," 1985.

[32] L. Hickey, J. Kloprogge, and R. Frost, "The effects of various hydrothermal treatments on magnesium-aluminium hydrotalcites," *Journal of Materials Science*, vol. 35, no. 17, pp. 4347-4355, 2000.

[33] R. Wang, X. Liang, Y. Peng, X.-w. Fan, and J.-x. Li, "Effect of the reaction temperature on nanocrystallites MgAl2O4 spinel ceramic precursor," in *J. Ceram. Proc. Res*, 2009, vol. 10, pp. 780-782.

[34] V. Rives, "Characterisation of layered double hydroxides and their decomposition products," *Materials Chemistry and Physics*, vol. 75, no. 1-3, pp. 19-25, 2002.

[35] G. Moradi, F. Khezeli, and H. Hemmati, "Syngas production with dry reforming of methane over Ni/ZSM-5 catalysts," *Journal of Natural Gas Science and Engineering*, vol. 33, pp. 657-665, 2016.

[36] S. Li and J. Gong, "Strategies for improving the performance and stability of Ni-based catalysts for reforming reactions," *Chemical Society Reviews*, vol. 43, no. 21, pp. 7245-7256, 2014.

[37] E. N. Kaufmann, "Characterization of Materials, 2 Volume Set," *Characterization of Materials, 2 Volume Set, by Elton N. Kaufmann (Editor), pp. 1392. ISBN 0-471-26882-8. Wiley-VCH, January 2003.*, p. 1392, 2003.

[38] N. E. Tsakoumis, A. P. York, D. Chen, and M. Rønning, "Catalyst characterisation techniques and reaction cells operating at realistic conditions; towards acquisition of kinetically relevant information," *Catalysis Science & Technology*, vol. 5, no. 11, pp. 4859-4883, 2015.

[39] U. Holzwarth and N. Gibson, "The Scherrer equation versus the'Debye-Scherrer equation'," *Nature nanotechnology*, vol. 6, no. 9, p. 534, 2011.

[40] S. Lowell, J. E. Shields, M. A. Thomas, and M. Thommes, *Characterization of porous solids and powders: surface area, pore size and density*. Springer Science & Business Media, 2012.

[41] C. N. Satterfield, "Heterogeneous catalysis in industrial practice," 1991.

[42] K. S. Sing *et al.*, "Reporting Physisorption Data for Gas/Solid Systems," *Handbook of Heterogeneous Catalysis: Online*, pp. 1217-1230, 2008.

[43] M. Thommes *et al.*, "Physisorption of gases, with special reference to the evaluation of surface area and pore size distribution (IUPAC Technical Report)," *Pure and Applied Chemistry*, vol. 87, no. 9-10, pp. 1051-1069, 2015.

[44] S. Bhatia, J. Beltramini, and D. Do, "Temperature programmed analysis and its applications in catalytic systems," *Catalysis Today*, vol. 7, no. 3, pp. 309-438, 1990.

[45] H. M. McNair and J. M. Miller, *Basic gas chromatography*. John Wiley & Sons, 2011.

[46] H. Tang, S. Li, D. Gong, Y. Guan, and Y. Liu, "Bimetallic Ni-Fe catalysts derived from layered double hydroxides for CO methanation from syngas," *Frontiers of Chemical Science and Engineering*, vol. 11, no. 4, pp. 613-623, 2017.

[47] G. Fornasari, M. Gazzano, D. Matteuzzi, F. Trifiro, and A. Vaccari, "Structure and reactivity of high-surface-area Ni/Mg/Al mixed oxides," *Applied Clay Science,* vol. 10, no. 1-2, pp. 69-82, 1995.

[48] H. Seo, "Recent scientific progress on developing supported Ni catalysts for dry (CO2) reforming of methane," *Catalysts,* vol. 8, no. 3, p. 110, 2018.

[49] D. Tichit, F. Medina, B. Coq, and R. Dutartre, "Activation under oxidizing and reducing atmospheres of Ni-containing layered double hydroxides," *Applied Catalysis A: General,* vol. 159, no. 1-2, pp. 241-258, 1997.

[50] D. Li, M. Koike, L. Wang, Y. Nakagawa, Y. Xu, and K. Tomishige, "Regenerability of hydrotalcite-derived nickel–iron alloy nanoparticles for syngas production from biomass tar," *ChemSusChem,* vol. 7, no. 2, pp. 510-522, 2014.

[51] L. E. Alzamora, J. R. Ross, E. C. Kruissink, and L. L. Van Reijen, "Coprecipitated nickel–alumina catalysts for methanation at high temperature. Part 2.—Variation of total and metallic areas as a function of sample composition and method of pretreatment," *Journal of the Chemical Society, Faraday Transactions 1: Physical Chemistry in Condensed Phases,* vol. 77, no. 3, pp. 665-681, 1981.

APPENDIX: CATALYST SYNTHESIS CALCULATIONS

Hydrotalcite- derived catalyst formula: $[M^{2+}_{1-x}M^{3+}_{x}(OH)_2]\ [(A^{n-}_{x/n})\cdot mH_2O]$

Catalyst after calcination and reduction: $Ni\text{-}Fe/MgO\text{-}Al_2O_3$

Where M^{2+} are a= mol of Ni^{2+} and c= mol of Mg^{2+}

M^{3+} are b=mol of Fe^{3+} and d= mol of Al^{3+}

- For $\frac{M^{2+}}{M^{3+}} = 3$, then $\Longrightarrow$ $\frac{a+c}{b+d} = 3$

The ratio of trivalent ion (x) to form hydrotalcite with good crystallinity must be in the range between 0.2 and 0.33.

For synthesis a value of x= 0.25 is chosen

$$x = b + d = 0.25$$

$$1 - x = a + c = 0.75$$

- Ni weight fraction: 20%

$$W_{Ni} = \frac{m_{Ni}}{m_{Ni} + m_{Fe} + m_{MgO} + m_{Al2O3}} = 20\%$$

$$W_{Ni} = \frac{a \times M_{Ni}}{a \times M_{Ni} + b \times M_{Fe} + c \times M_{MgO} + \left(\frac{d}{2}\right) \times M_{Al2O3}} = 20\%$$

- The molar ratio of $\frac{Fe}{Ni} = 0.1$, is called R

$$\frac{n_{Fe3+}}{n_{Ni2+}} = \frac{b}{a} = R = 0.1$$

- b, c and d can be replaced in terms of a from previous equations

  b= R x a c= 0.75-a d= 0.25 – (R x a)

$$\frac{a \times M_{Ni}}{a \times M_{Ni} + (R \times a) \times M_{Fe} + (0.75\text{-}a) \times M_{MgO} + \left(\frac{0.25\text{-}(R \times a)}{2}\right) \times M_{Al2O3}} = 20\%$$

Solving equation for (a) we have

$$a = \frac{a \times M_{Ni}}{a \times M_{Ni} + (R \times a) \times M_{Fe} + (0.75\text{-}a) \times M_{MgO} + \left(\frac{0.25\text{-}(R \times a)}{2}\right) \times M_{Al2O3}}$$

$$a = \frac{0.15 \times M_{MgO} + 0.025 \times M_{Al2O3}}{0.8 \times M_{Ni} + 0.02 \times M_{Fe} + 0.2 \times M_{MgO} + 0.01 \times M_{Al2O3}}$$

With the value of (a), all the stochiometric coefficients can be found

$$OH^{-1} = 2 \times (a+b+c+d)$$

$$CO_3^{2-} = \frac{\left(2x(a+c)\right)+\left(3x\,(b+d)\right)-OH^{-1}}{2}$$

The mole of reactant is calculated with the stochiometric coefficients for a metal concentration of 100 mL, metal nitrate solution was 0.25 M. Results are presented in table A.1

Table A.1 Stochiometric coefficients and mole of reactants of hydrotalcite-derived catalyst

Reactants	Stochiometric coefficients	Mole of reactant
Ni^{2+}	0.156	0.004
Fe^{3+}	0.016	0.0004
Mg^{2+}	0.594	0.0148
Al^{3+}	0.234	0.0059
OH^-	2.000	0.0050
CO_3^{2-}	0.125	0.003

Finally, the mass of reactants can be calculated using the mole of reactants and their molecular weight, one equivalent of Na_2CO_3 was added in excess to ensure pillaring. Results are presented in table A.2

Table A.2 mass and molecular weight of reactants used for catalyst synthesis

Reactants	Mass of reactants (g)	Molecular weight (g/mol)
$Ni(NO_3)_2 \cdot 6H_2O$	1.1378	290.81
$Fe(NO_3)_3 \cdot 9H_2O$	0.1580	402.95
$Mg(NO_3)_2 \cdot 6H_2O$	3.8045	256.41
$Al(NO_3)_3 \cdot 9H_2O$	2.1978	375.13
NaOH	2.0000	40.00
Na_2CO_3	0.6624	105.99